Biomedicine & Pharmacotherapy 194 (2026) 118902

Contents lists available at ScienceDirect

Biomedicine & Pharmacotherapy

journal homepage: www.elsevier.com/locate/biopha

Treatment with a botanical mixture of cannabidiol:Δ^9-tetrahydrocannabinol enhances microglial phagocytosis and shapes amyloid plaques in a mouse model of Alzheimer's disease

Samuel Ruiz de Martín Esteban [a], M. Teresa Grande [a], Ana M. Martínez-Relimpio [a], Diego Herráez-Aguilar [a], Ricardo Mostany [b], Cecilia J. Hillard [c], William H. Hind [d], Julián Romero [a,*]

[a] Faculty of Experimental Sciences, Universidad Francisco de Vitoria, Pozuelo de Alarcón, Madrid 28223, Spain
[b] Department of Pharmacology, Tulane University School of Medicine, New Orleans, LA 70112, USA
[c] Neuroscience Research Center and Department of Pharmacology and Toxicology, Medical College of Wisconsin, Milwaukee, 53226, WI, USA
[d] Jazz Pharmaceuticals, Sovereign House, Vision Park, Cambridge, CB24 9BZ, UK

ARTICLE INFO

Keywords:
Alzheimer's disease
Amyloid plaque
Microglia
Phagocytosis

ABSTRACT

The potential use of phytocannabinoids in neurodegenerative disorders is currently under intense investigation based on their potential anti-inflammatory, antioxidant, and neuroprotective effects. Here, we tested the effects of chronic (28 days) treatment with a complex botanical mixture of purified cannabidiol:Δ^9-tetrahydrocannabinol (CBD:THC, 99:1) in male 5xFAD mice, a murine model of Alzheimer's disease that recapitulates amyloid pathology. Effects of exposure to this cannabinoid mixture were evaluated using behavioral tests (elevated plus maze for anxiety, tail suspension for depression-like behavior, rotarod for motor coordination, open field for locomotor activity, and novel object recognition for memory), quantification of protein expression (IL-1β, CD40, TREM2, COX2), assessment of functional parameters (microglial phagocytic activity by flow cytometry), and *in vivo* multiphoton microscopy (time-course of changes of neuritic plaque structural features). Twice daily dosing with 50 mg/kg subcutaneously (s.c.) significantly reduced locomotion, increased anxiety- and depression-like behaviors and had no effect on memory and motor coordination. *In vivo* imaging experiments suggest that the CBD:THC treatment enhanced microglial phagocytic activity on amyloid plaques; this effect was observed both in plaque features (multiphoton microscopy measurements) as well as in microglia (flow cytometry data). Exposure to CBD:THC induced significant changes in *in vivo* microglia-amyloid interactions, increasing phagocytic activity and reducing the amyloid peptide accumulation in the neuritic plaques. Thus, CBD:THC (99:1) may be a promising treatment to reduce amyloid pathology, though caution should be noted due to the behavioral alterations observed, i.e., increased anxiety- and depression-like behaviors as well as decreased locomotion.

1. Introduction

The term "phytocannabinoid" refers to a series of compounds produced by the *Cannabis sativa* plant and comprises several hundred chemical entities [26,53]. The two best studied phytocannabinoids to date are Δ^9-tetrahydrocannabinol (THC) and cannabidiol (CBD) and their potential therapeutic use, either separate or combined, is currently under intense scrutiny in several disease conditions [44]. One of the diseases in which the use of these cannabinoids is being studied is Alzheimer's disease (AD) [18]. This neurodegenerative disorder is the most prevalent cause of dementia worldwide and its incidence is expected to grow in the years to come as a consequence of the increase in life expectancy of advanced societies. Most of the AD cases are "sporadic", that is, of unknown etiology, while a very low number of them are of genetic origin [40].

Recent literature highlights the potential relevance of the use of CBD and THC for the treatment of AD through the interaction with CB1 and CB2 receptors for THC [1,18], and probably with other additional targets, such as glycine receptors (for THC), or GPR55, 5-HT_{1A}, TRPV1, and $GABA_A$ (for CBD) [68]. Different mouse models of this disease have been

* Corresponding author.
E-mail address: j.romero.prof@ufv.es (J. Romero).

https://doi.org/10.1016/j.biopha.2025.118902
Received 1 August 2025; Received in revised form 27 November 2025; Accepted 8 December 2025
Available online 12 December 2025

used to study these effects *in vivo*; short-term (1–2 weeks) administration of CBD (0,5–10 mg/kg) to amyloid β (Aβ)-injected mice, as well as long-term (6–8 months), oral administration of CBD (20 mg/kg), led to improvements in several aspects of the disease, including behavioral deficits (cognitive function, social recognition, spatial learning), and neuroinflammation (cytokine production, glial activation) [15,16,23,45]. Interestingly, Watt et al. [73] used a higher dose of CBD (50 mg/kg, i.p.) in 12-month-old mice and found improvements in social recognition and spatial memory that were not accompanied by any benefit in terms of neuroprotection or antiinflammation, highlighting the relevance of age and dose in these types of studies [73].

Regarding THC, Chen et al. [14] administered it at several doses (1–30 mg/kg) to 5xFAD mice and demonstrated that the deleterious effects associated with exposure to this cannabinoid (loss of synapses and memory impairment) were mediated by a CB_1-induced increase in cyclooxygenase-2 (COX-2) expression. Importantly, THC also produced beneficial effects in these mice (amyloid burden reduction and prevention of neurodegeneration), and these effects were maintained even after COX-2 inhibition [14]. Very recently, Wang et al. [72] have studied the effects of a 3-month treatment with low doses of THC (0.02 and 0.2 mg/kg) in APP mice and found a dose-dependent improvement in spatial memory that was accompanied by a decrease in amyloid oligomers [72].

It is important to note that only a few studies have employed combinations of CBD:THC to explore their potential therapeutic interest in AD. It has been known for decades that CBD may dampen or enhance the effects of THC both in humans as well as in rodents, with the dose and route of administration as key factors for such interactions [68]. A seminal study by Casarejos et al. [13] revealed that chronic (one month) treatment with Sativex (a complex botanical mixture, with a 1.08:1 mixture of THC and CBD as its principle cannabinoid constituents) induced a decrease in tau and amyloid protein precipitates in a mouse model of tauopathy [13]. An *in vitro* study by Janefjord et al. [34] showed that neither THC nor CBD modified the morphology of amyloid aggregates [34]. In addition, while CBD provided direct neuroprotection to cultured neurons (SH-SY5Y), THC did not. Interestingly, both CBD and THC prevented neuronal damage when added to LPS-activated BV2-conditioned media, suggesting a role for microglia and a putative receptor-independent effect of these cannabinoids. Aso et al. [7] found that exposure to plant extracts containing CBD (0.75 mg/kg), THC (0.75 mg/kg), or a combination of both (1:1) preserved memory in the APP/PS1 mouse model of AD, but only when administered in the early symptomatic phase of the disease [7]. Using the same animal model, these authors have very recently reported that a five-week treatment with CBD:THC (0.5 mg/kg each) reduced extracellular levels of glutamate in the hippocampus, most probably by modulating astrocytic uptake, which could exert a relevant anti-excitotoxic effect [61].

We have recently described the effects of a low dose of synthetic CBD (0.273 mg/kg), of THC (0.205 mg/kg), and of a combination of both, in the 5xFAD model of AD [5]. We found that insoluble amyloid levels were increased in all cases, pointing to an effect of these cannabinoids on the processing and/or deposition of this pathological peptide. In addition, we found that mice exposed to a combination of CBD:THC, but not to each cannabinoid separately, showed a significant improvement in spatial memory. These effects were not accompanied by changes in the expression levels of markers of neuroinflammation.

The 5xFAD mouse model recapitulates most of the neuroinflammation-associated features of AD, including gliosis, amyloid peptide accumulation, and cytokine production [27,50,51]. This mouse line contains five mutations of familial AD (APP K670N/M671L (Swedish); I716V (Florida); V717I (London); PS1 M146L; and L286V) and is characterized by an exacerbated production of Aβ 1–42 and 1–40 as well as by the early appearance of neuritic plaques, as early as at 3 months of age, which makes this mouse model an appreciated tool to study amyloid-associated neuroinflammation. Neuronal loss and myelin abnormalities are also reported from 6-month-old 5xFAD mice [50] and some studies reported impaired memory and motor coordination in 9-month-old mice [25,27].

In the present study we looked at the effects of a complex botanical mixture of purified phytocannabinoids (CBD:THC; 99:1) on *in vivo* features of amyloid pathology in the 5xFAD mouse model of AD. Behavioral tests on memory, anxiety, depression, and motor activity were employed and combined with molecular analysis of the neuroinflammatory response and of the phagocytic activity of microglial cells and with the assessment of the time-course of amyloid-microglial interactions by *in vivo* multiphoton microscopy.

2. Experimental procedures

2.1. Study animals

Male mice co-expressing five familial AD mutations (5xFAD) on a C57BL6/J background were purchased from Jackson Laboratories (Bar Harbor, ME, USA; [50] and were mated with $CB_2^{EGFP/f/f}$ mice [42] and backcrossed for at least 5 generations to generate $CB_2^{EGFP/f/f}$/5xFAD mice. Breeding scheme was always performed so that the transfer of the transgene occurred only through the paternal germ line [65]. Animals employed in the present experiments were 3, 6, and 9 months old at the start of the experiments. This period was chosen based on previously published data [50,70] to allow for the appearance of amyloid deposits and phenotypic alterations and to study different phases of the disease. Mice were housed in the animal facility of Universidad Francisco de Vitoria (authorization number #281150000013). Experimental protocols were followed according to European and Spanish regulations for protection of experimental animals (2010/63/EU and RD 1201/2005 and 53/2013) and were authorized by the local ethics committee (PROEX149/18).

2.2. Drugs and administration regime

Plant-derived, highly purified CBD (batch number GRN170047 (6062849), 99.1 % purity by HPLC) and THC (batch number THC100513, 96.4 % purity by HPLC) were supplied by GW Research Ltd UK (now Jazz Pharmaceuticals Research Ltd UK), stored at −20°C, protected from light, and formulated in vehicle (veh) of Cremophor® EL: Ethanol:saline (in a 1:2:17 ratio). Injectable solutions were prepared fresh each day and were continuously stirred until injection.

A CBD:THC mixture (99:1 ratio) was administered subcutaneously twice daily for 28 consecutive days, at total doses of 50 mg/kg or 100 mg/kg of the mixture [54]. These correspond to 49.5 mg/kg CBD + 0.5 mg/kg THC and 99 mg/kg CBD + 1 mg/kg THC, respectively. Injection volumes were adjusted to body weight (5 μL per g), and the injection sites were rotated between the neck, right flank, and left flank to minimize local tissue irritation. *In vivo* exposure to 100 mg/kg of a CBD:THC (99:1) twice daily, s.c., led to the formation of subcutaneous abscesses after day 28 in several 9-month-old mice, and consequently, this dose was terminated in all groups of mice. Only data relating to the 50 mg/kg twice daily dose are reported here.

2.3. Experimental designs

Two experimental paradigms were employed. In the first one (behavioral studies), 5xFAD mice were treated with 50 mg/kg CBD:THC (99:1), s.c., twice per day, for 28 days and subjected to several behavioral tests during the course of the treatment (see Fig. 1A). At the end of the treatment period mice were humanely killed and their brains removed immediately after, then frozen on dry ice, and stored at −80°C for molecular biology determinations.

In the second set of experiments (multiphoton microscopy), a cranial window was implanted on 5xFAD/$CB_2^{EGFP/f/f}$ mice and treated with 50 mg/kg CBD:THC (99:1), s.c., twice per day, for 28 days. During the treatment period mice were subjected to an imaging session in a

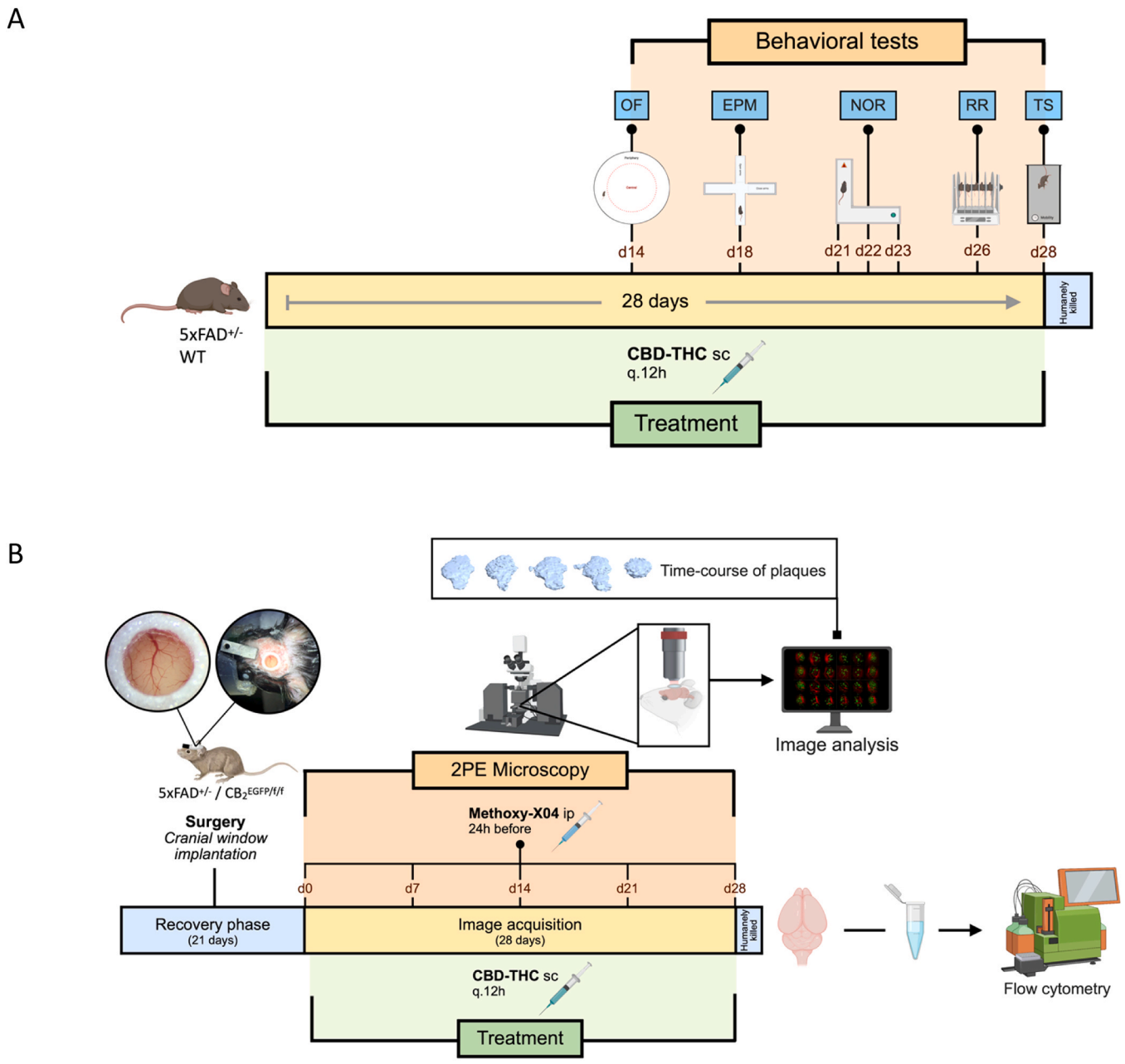

Fig. 1. Graphic summary of 50 mg/kg CBD:THC (99:1) treatment, behavioral studies, and use of tissue samples (A), and of *in vivo* multiphoton imaging sessions, and use of tissue samples (B). In a first set of experiments (A), 5xFAD mice were treated with 50 mg/kg CBD:THC (99:1), s.c., twice per day, for 28 days and subjected to a battery of behavioral tests during the course of the treatment; these included locomotor activity (open field test, OF, day 14), anxiety-like behavior (elevated plus maze, EPM, day 18), memory (novel object recognition test, NOR, days 21–23), motor control (rotarod, RR, day 26), and depression-like behavior (tail suspension test, TS, day 28). (B) Multiphoton microscopy was used to perform a time-course analysis of the progression of amyloid plaques in 6-month-old mice exposed to vehicle or CBD:THC. Parameters measured included plaque volume, complexity, fluorescence intensity and density.

multiphoton microscope once a week and a time-course analysis of amyloid plaque evolution was performed *in vivo*. At the end of the treatment mice were humanely killed and their brains processed for flow cytometry determinations (see Fig. 1B).

2.4. Behavioral studies

Several behavioral tests were employed to investigate the effects of the 28-day chronic dosing of CBD:THC on anxiety-like (elevated plus maze, EPM) and depression-like (tail suspension) behaviors, as well as on motor control (rotarod, RR), locomotor activity (open field test, OF), and memory (novel object recognition test, NOR) end-points. We followed protocols previously described by us [70] or by other groups [11,37,41,43,63,64,66]. The sample sizes for each end-point are shown in Table 1. See supplementary information for details on the tests used.

Several behavioral tests were employed to investigate the effects of the 28-day chronic dosing of CBD:THC on locomotor activity (open field test, OF, day 14), anxiety-like behavior (elevated plus maze, EPM, day 18), memory (novel object recognition test, NOR, days 21–23), motor control (rotarod, RR, day 26), and depression-like behavior (tail suspension test, TS, day 28). We followed protocols previously described by us [70] or by other groups [11,37,41,43,63,64,66]. The sample sizes for each end-point are shown in Table 1. See supplementary information for details on the tests used.

Table 1
Sample size per group and treatment in behavioral studies.

	VEH-3MO	CBD:THC-3MO	VEH-6MO	CBD:THC-6MO	VEH-9MO	CBD:THC-9MO
EPM	9	5	76	6	6	7
Tail suspension	8	8	9	9	8	9
NOR	100	8	9	10	5	6
Rotarod	10	10	10	10	9	10
Open field	8	10	10	11	8	9

2.5. $A\beta_{1-42}$ ELISA

To determine $A\beta_{1-42}$ levels in the hippocampus, tissues were homogenized in 10 volumes of ice-cold guanidine buffer (5.0 M guanidine·HCl/50 mM Tris·Cl, pH 8.0) containing protease inhibitor cocktail (Roche). Protein concentrations were determined by BCA assay (Thermofisher). Human ELISA kits (Invitrogen) were used according to manufacturer's specifications. Optical signals at 450 nm were read on a Sunrise microplate reader (Tecan) and sample concentrations were determined by interpolation using the respective standard curves.

2.6. Western blot

We analyzed the expression levels of several neuroinflammation-related markers by western blot; these proteins included cytokine IL1β, CD40 and TREM2 cell receptors, and cyclooxygenase-2 isoenzyme (COX-2). All these proteins are known to participate in relevant aspects of amyloid pathology such as inflammation, phagocytosis, or microglial cell activity [4,74].

Brain cortices were separated and homogenized in lysis buffer (25 mM HEPES pH 7.5, 150 mM NaCl, 1 % Igepal CA-630, 10 mM $MgCl_2$, 1 mM EDTA, supplemented with 10 % glycerol, 10 μg/mL aprotinin, 10 μg/mL leupeptin, 100 mM PMSF, 25 mM NaF, and 1 mM Na_3VO_4. Samples were centrifuged at 14.000 x g for 30 min and supernatant was recovered and proteins were quantified. Tissue lysates (60 μg/lane) were loaded onto SDS-polyacrylamide gels, and the proteins were transferred onto PVDF membranes (BioRad). After blocking in TTBS (10 mM Tris pH 7.5, 150 mM NaCl, 0.1 % Tween 20 plus 2 % bovine serum albumin) membranes were incubated overnight at 4ºC, as appropriate, with: anti-amyloid precursor protein (APP; 1:1000, MAB348, clone 22C11, Sigma-Aldrich), anti-β-actin (1:5000, Sigma), anti-CD40 (1:1000, ThermoFisher – Invitrogen), anti-COX-2 (1:200, Santa Cruz Biotechnology), or anti-TREM2 (1:1000, ThermoFisher-Invitrogen). Membranes were incubated with the corresponding horseradish peroxidase-conjugated secondary antibody (1:10,000) and were developed using a chemiluminescent reagent (ECL detection reagent GE Healthcare). Developed signals were recorded on ChemiDoc Imaging System (BioRad) for densitometric analysis (ImageJ, NIH, MD, USA). In some cases, a mild membrane stripping protocol was performed to allow the investigation of various proteins on the same blot, particularly when molecular weights were very similar. Briefly, membranes were incubated at room temperature for 5–10 min with a mild stripping buffer (1.5 % glycine, 0,1 % SDS and 1 % Tween20 in distilled water pH 2.2). Buffer was discarded and incubation with stripping buffer was repeated. Then, membranes were washed twice for 10 min in PBS, then washed twice for 5 min in TTBS and were again incubated with blocking TTBS solution. ECL detection reagent was used to determine the membrane stripping efficiency and no signal bands should be detected if the primary antibody was successfully removed.

2.7. In vivo multiphoton microscopy

We also performed a longitudinal assessment of plaque evolution in parallel to the treatment with CBD:THC by *in vivo* multiphoton microscopy (Fig. 1B). At the end of the experiment, the phagocytic activity of microglia was quantified by flow cytometry.

Six-month-old mice ($N = 4–5$ per group) were subjected to a surgical procedure in order to implant a cranial window that, without affecting the meninges, granted direct visualization of the brain parenchyma by multiphoton (MPT) microscopy [21,31,48,71]. The surgical procedure was as follows: mice were deeply anesthetized with isoflurane and secured to a stereotaxic frame. After removing the skin and muscle, the cranial surface was exposed. A cranial window (3 mm in diameter) was opened with a high-speed drill. The brain tissue was kept humid throughout the whole procedure by frequent additions of warm saline solution. The window was then covered with a glass coverslip and sealed. Mice were constantly monitored and allowed to recover in individual cages for three weeks. After this recovery period, mice were started in a regimen of five imaging sessions, one week apart (Fig. 1B). To visualize amyloid plaques, mice received i.p. injections of methoxy-X04 (10 mg/kg), 24 h before the imaging session [39]. This strategy allowed for the direct visualization of individual amyloid plaques (10–12 per mouse) and time-course analysis of their size as the treatment progressed.

Before every imaging session, mice were anesthetized with isoflurane (5.0 % for induction, 1.5 % for imaging) and secured to a custom-built 2PE microscope using a titanium bar. Imaging was done using a Ti:sapphire laser (Chameleon Ultra II; Coherent) and ScanImage software written in MATLAB [55]. First, under bright light illumination and using a 4x objective (Olympus UPLFLN 4x/0.13), cortical surface images were acquired to orient and locate the regions of interest (ROIs) using the vascular pattern as landmarks. Second, excitation of methoxy-X04 was achieved at 800 nm with a two-photon excitation laser, limiting the power at the sample to < 20 mW. A 40X water immersion objective (Olympus LUMPLFLN 40x/0.80) was used to create a map of the ROI and identify the position of plaques at low magnification (0.36 μm/pixel), followed by the acquisition of image stacks of individual plaques at high magnification (0.18 μm/pixel). Amyloid plaques (10–20 from 2 to 3 ROIS per mouse) were imaged at a minimun depth of 100 mm in the brain parenchyma and their x, y, and z coordinates recorded to locate the same amyloid plaques in subsequent image sessions.

2.8. Image analysis

Images acquired by multiphoton microscopy were processed using a custom pipeline implemented in *Wolfram Mathematica* 14.0 (Wolfram Research, Inc., Mathematica, Version 14.0, Champaign, IL) (Fig. 2). Three-dimensional reconstruction began by stacking the individual 2D slices, assigning voxel dimensions consistent with the microscope's spatial resolution along the *xyz* axes. The intensity dynamic range was normalized to the [0,1] interval, and Gaussian smoothing (kernel radius $r = 3$) was applied to reduce speckle noise while preserving object boundaries. Segmentation of amyloid plaques was performed using Otsu's variance maximization method [52], followed by morphological filling of internal minima (Wolfram Research, Inc.). The resulting binary masks were converted into 3D surface meshes via the Dual Marching Cubes algorithm [49], enabling volumetric quantification. For each identified component $\mathscr{R}_i(x,y,z)$, the enclosed volume V_i was computed by numerical integration over the region of interest, and the largest connected component was selected for subsequent analysis. The segmented 3D region was then used to mask the original intensity image

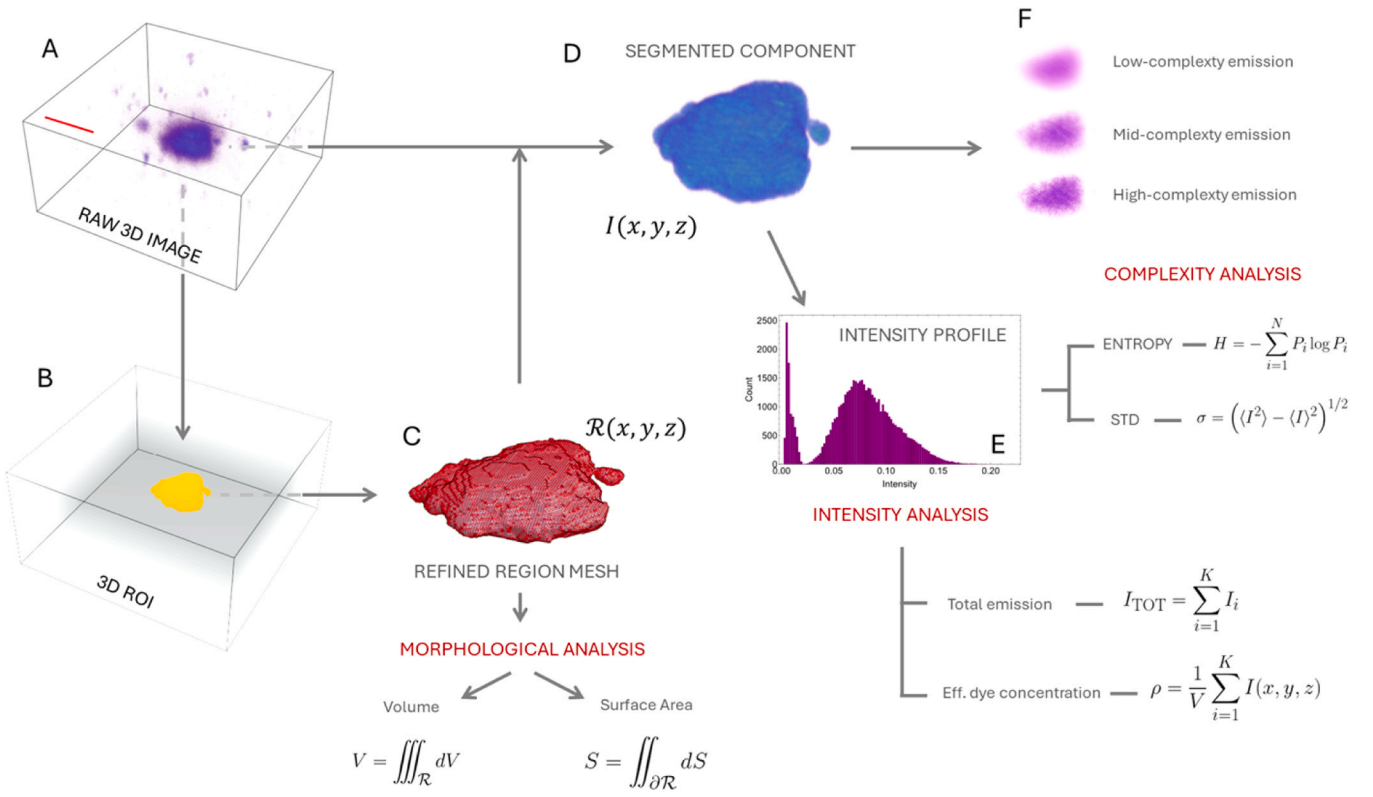

Fig. 2. Workflow for 3D image reconstruction and structural complexity analysis of amyloid plaques. (A) Raw 3D image acquired by multiphoton confocal microscopy. (B) 3D region of interest (ROI) obtained after Gaussian smoothing (r = 3), Otsu thresholding, and hole filling to ensure topological continuity of the segmented region. (C) 3D mesh reconstruction of the ROI using the Dual Marching Cubes algorithm, providing a refined geometrical representation of the plaque surface. The resulting mesh enables quantitative estimation of plaque volume and surface area. (D) Segmented image element obtained by applying the 3D ROI as a mask on the original intensity data. (E) Fluorescence emission profile computed within the ROI, yielding the total fluorescence intensity and fluorophore density which reflect the integrated and normalized concentration of dye molecules, respectively. Complexity analysis performed from the fluorescence intensity distribution, using intensity entropy and standard deviation of voxel intensities as complementary indicators of heterogeneity. Entropy quantifies the disorder of the fluorescence distribution, while STD captures the magnitude of local intensity fluctuations. (F) Representative examples of plaques with different emission complexity: (a) low-entropy, homogeneous emission; (b) intermediate-entropy plaque showing moderate heterogeneity; and (c) high-entropy plaque exhibiting pronounced textural irregularity and structural complexity.

for quantitative fluorescence measurements.

Under the assumption of a linear fluorescence response, valid for low fluorophore concentrations and moderate excitation intensities, the detected signal I_f is expected to scale proportionally with the number of emitting molecules within the illuminated region $\mathscr{R}_i$. This relationship can be expressed as $I_f = k \cdot N_f \cdot I_0$

where I_0 is the local excitation intensity, N_f is the number of fluorophores contributing to emission, and k is a proportionality constant encompassing factors such as the fluorophore's absorption cross-section, quantum yield, optical collection efficiency, and detector gain. Within this linear regime, the measured fluorescence intensity provides a direct, quantitative proxy for the concentration of labeled molecules. This approximation is valid if the local fluorophore concentration remains below the threshold where inner filtering, self-quenching, or saturation effects become significant. Under these conditions, fluorescence emission scales linearly with the amount of bound dye, and variations in measured intensity across the 3D image primarily reflect spatial differences in fluorophore density rather than nonlinear optical artifacts.

From this physical basis, several quantitative descriptors were derived to characterize the fluorescent amyloid plaques. The total plaque intensity I_{TOT} was defined as the sum of voxel intensities within the segmented 3D region, $I_{TOT} = \sum_{xyx\in\mathscr{R}} I(x,y,z)$, which represents the integrated fluorescence emitted by all fluorophores contained within the plaque volume. This metric thus reflects both the overall amount of labeled protein and the total emitting volume. In contrast, the fluorescence density, defined as $\rho = I_{TOT}/V$ provides a normalized measure of average fluorophore concentration, decoupling intrinsic biochemical differences from geometric effects. Because this ratio accounts for the volumetric extent of the plaque, it enables direct comparison between plaques of distinct sizes or morphologies. High values of ρ indicate densely labeled regions with high fluorophore packing or local enrichment of amyloid fibrils, whereas low ρ values are characteristic of more diffuse or weakly labeled aggregates.

Together, I_{TOT} and ρ provide complementary measures: the former quantifies the total optical output of the plaque, while the latter isolates concentration-dependent variations independent of plaque volume. These intensity-based parameters form the foundation for subsequent analyses of fluorescence heterogeneity and complexity, which are further assessed through the entropy-based texture descriptors described below.

To characterize spatial heterogeneity and textural complexity within segmented amyloid plaques we computed the intensity (Shannon) entropy for each three-dimensional region. The entropy was calculated from the empirical (normalized) intensity distribution $P(I_i)$ within a region ($\mathscr{R}$) as $H = -\sum_{i=1}^{K} P(I_i)\log P(I_i)$ where I_i denotes the $i-th$ intensity bin, K the number of bins. $P(I_i)$ is obtained by counting voxels per bin and normalizing by the region voxel count $N = \sum_i n_i$.

The theoretical maximum entropy for a distribution over K discrete levels is $H_{Max} = \log K$, which occurs when the intensity histogram is uniform. Importantly, $H_{\max}$ depends only on K (the number of intensity levels or histogram bins) and not on the number of voxels (N) in the region. Because all ROIs in this study were acquired with identical im-

aging bit depth and dynamic range and were processed using the same rescaling protocol, K was held constant across regions; therefore, entropy values are directly comparable between ROIs regardless of their volume. For presentation and easier interpretation, we also report the normalized entropy $H_{rel} = H/H_{max}$ which quantifies the fraction of the maximum possible uncertainty captured by the observed intensity distribution.

The proposed entropy estimator H is known to be biased downward for finite samples. However, when the number of voxels in each segmented plaque exceeds the number of occupied bins $N \gtrsim K$, this bias is assumed to be small enough.

Entropy quantifies the statistical heterogeneity of voxel intensities within a plaque and therefore provides a useful proxy for textural complexity. Low entropy indicates a narrow, concentrated intensity distribution. Biologically, this reflects homogeneous fluorophore labeling and, by implication, relatively uniform packing or composition of amyloid material within the plaque. Texturally, such regions appear optically smooth and structurally ordered. High entropy indicates a broad intensity distribution with multiple intensity modes or substantial dispersion. This may arise from local fluctuations in dye binding, variations in fibril packing density, presence of subdomains with different refractive properties, or partial penetration of stain. Texturally, high-entropy plaques manifest greater internal complexity, inhomogeneous labeling, or substructural heterogeneity.

To complement the entropy-based analysis, we also quantified fluorescence heterogeneity using the standard deviation (σ_I) of voxel intensities within each ROI. The STD Intensity provides an amplitude-based measure of heterogeneity, directly reflecting the magnitude of fluctuations in fluorescence emission. While entropy captures the complexity of the intensity distribution (e.g., whether it is uniform, multimodal, or skewed), the STD captures the *extent* of intensity variation. Thus, regions with high σ_I exhibit strong contrast gradients or heterogeneous labeling, whereas regions with low σ_I display optical uniformity. The combined interpretation of H and σ_I enhances sensitivity to subtle differences in plaque organization: for example, a plaque may exhibit high STD but moderate entropy if it contains two dominant subregions with distinct but internally homogeneous intensities, whereas a plaque with similar STD but higher entropy may present a continuum of local intensity variations, reflecting more intricate substructure.

Entropy and STD therefore serve as complementary descriptors of textural organization, linking optical heterogeneity to the nanoscale molecular disorder of amyloid aggregates. In this framework, entropy represents the informational complexity of the fluorophore distribution, whereas STD quantifies its overall variability, allowing a multiparametric assessment of plaque structure beyond mean intensity or volume measurements.

2.9. In vivo phagocytosis assay

The day before being humanely killed, mice received a single injection, i.p., of methoxy-X04 (10 mg/kg) to fluorescently label amyloid-enriched neuritic plaques and amyloid ingested by microglial cells. Brain tissue was dissociated, and microglial cells were obtained by Percoll (GE Healthcare) density gradient centrifugation and cells were stained with CD11b-PE and CD45-APC-Vio770 antibodies (Miltenyi Biotec). Debris and cell aggregates were removed from the analysis using forward and side scatter characteristics, and CD11b+ and CD45lo populations were identified as microglial cells as previously described [3]. Samples were read on a MACSQuant Flow Cytometer and analyzed with MACS Quantify software (Miltenyi Biotec). Fluorescence signals were corrected by fluorescence minus one (FMO) control [3].

2.10. Statistical analyses

Data were analyzed with GraphPad Prism software (version 10.3.0; San Diego, CA, USA). All data were tested for normality using d'Agostino-Pearson or Shapiro–Wilk for data where there are identical values for different samples and/or $n < 8$. All normal data were assessed for outliers (ROUT in Prism) and any outliers were removed for subsequent analysis. Data are expressed as mean ± standard error of the mean (SEM). Statistical analyses were made using two-tailed Student-*t*-test (flow cytometry data) or two-way analysis of variance followed by Sidak's post-hoc test. A p value < 0.05 was considered as statistically significant.

3. Results

3.1. Behavioral data

3.1.1. Elevated plus maze

Both vehicle- and CBD:THC-treated 5xFAD mice spent more time in the open arms of the EPM as a function of the age of the animals (Fig. 3A), indicative of an age-related reduction in anxiety-like behavior [$F(2,34) = 22.46$, $p < 0.0001$]. Vehicle-treated mice spent a significantly higher percentage of the time in the open arms of the EPM at 6 and 9 months of age compared with 3-month-old mice ($p = 0.0181$ and $p < 0.0001$, respectively); CBD:THC-treated mice exhibited a significant increase in the percentage of time spent in the open arm at 9 months of age, compared with mice of 3 and 6 months of age ($p = 0.0003$ and $p = 0.0005$, respectively). Regarding the treatment, no significant changes were found [$F(1,34) = 2.603$, $p = 0.1159$].

3.1.2. Tail suspension test

There were no changes in the time spent immobile due to age [$F(2, 45) = 0.4350$, $p = 0.6500$] or treatment [$F(1, 45) = 0.4381$, $p = 0.5114$], with a significant interaction between both factors [$F(2, 45) = 4.681$, $p = 0.0142$] (Fig. 3B).

3.1.3. Novel object recognition test

There was no change in the ratio of exploration time due to age [$F(2, 42) = 0.3723$, $p = 0.6914$] or treatment at any age [$F(1, 42) = 0.1533$, $p = 0.6974$], nor in the interaction between factors [$F(2, 42) = 2.414$, $p = 0.1018$] (Fig. 3C).

3.1.4. Rotarod

Three trials per mouse were carried out. As expected, the latency to stay on the rod significantly increased over successive trials. At 3 months of age, no differences were found due to the treatment [$F(1, 50) = 0.8136$, $p = 0.3714$] and a significant effect of trial was shown [$F(2, 50) = 7.815$, $p = 0.011$] (Fig. 3D, left). There were significant differences within each treatment group at 6 months of age [$F(2, 50) = 12.48$, $p < 0.0001$], and no differences were found due to the treatment [$F(1, 50) = 1.539$, $p = 0.2206$] (Fig. 3D, center). Finally, at 9 months of age, a significant difference was found considering the main factor trial [$F(2, 50) = 9.242$, $p = 0.0004$], with no changes associated to the main factor treatment [$F(1, 50) = 1.731$, $p = 0.1943$] (Fig. 3D, right). Overall, CBD:THC treatment had no effect on mice performance on the rotarod test.

3.1.5. Open field test

CBD:THC treatment had no effect on the amount of time mice spent in the central part of the arena (Fig. 4A; [$F9(1, 50) = 1.261$, $p = 0.2668$]); however, a significant effect of the main factor age was detected [$F(2, 50) = 12.91$, $p < 0.0001$] with no interaction between factors [$F(2, 50) = 0.2110$, $p = 0.8105$]. Post-test analysis revealed significant increases in the time spent in the central area of the arena in 6- and 9-month-old mice compared to the 3-month-old mice in both treatment groups (Fig. 4A). In addition, and while drug treatment had no effect on the time spent in the periphery of the arena [$F(1, 50) = 2.096$, $p = 0.1539$], a significant main effect was evident due to age [$F(2, 50) = 12.53$, $p < 0.0001$], but not the interaction between age and treatment factors [$F(2,50) = 0.07844$, $p = 0.9247$]. Post-hoc analysis

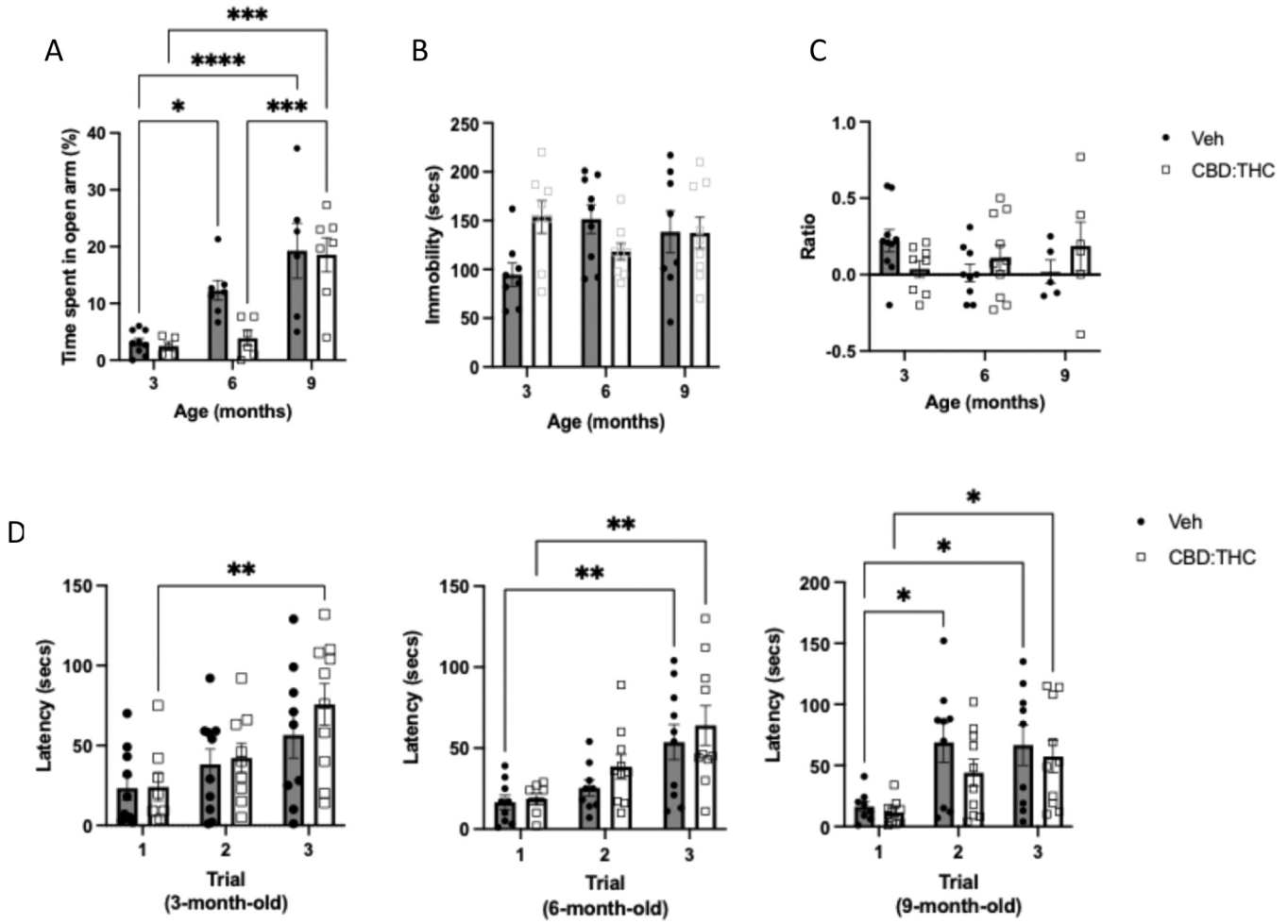

Fig. 3. Assessment of anxiety-like behavior (A), depression-like behavior (B), memory impairments (C), and motor coordination (D) in 5xFAD mice exposed to subcutaneous administration of vehicle or CBD:THC 50 mg/kg, for 28 days. Assessments were done 2 h after the CBD:THC (99:1) administration. Each data point represents individual values for each mouse. (A) Anxiety-like behavior was assessed by the elevated plus maze and was reduced in older mice; exposure to cannabinoids induced a pro-anxiogenic effect in 6-month-old mice. N = 5–9 mice per group. (B) Time spent in immobility during tail suspension for 6 min. Treatment with CBD:THC led to an increase in depression-like behavior in 3-month-old mice and also increased with age (6- vs 3-month-old) in vehicle-treated animals. N = 8–9 mice per group. (C) Memory performance measured by the novel object recognition test showed no changes due to age or treatment. N = 6–10 per group and treatment. (D) Motor coordination measured with the rotarod test in 5xFAD mice. Latency to fall from the rotarod increased with repeated trials in the test at 3 (left), 6 (middle), and 9 (right) months, while no effects associated with the treatment were found. N = 9–10 mice per group. Data shown as mean ± SEM. Two-way ANOVA followed by Sidak's post-hoc test; *p < 0.05, **p < 0.01, ***p < 0.001, ****p < 0.0001.

revealed that 6- and 9-month-old mice from the drug and vehicle-treated groups spent significantly less time in the periphery compared to 3-month-old mice (Fig. 4B).

Regarding locomotion, treatment with CBD:THC significantly reduced the total distance covered by mice [$F(1, 48) = 19.09$, $p < 0.0001$], with significant differences between treatment groups at 3, 6, and 9 months of age ($p = 0.0118$, $p = 0.0499$ and $p = 0.0056$, respectively) (Fig. 5A). CBD:THC-treated mice traveled less distance in the central part of the arena [$F(1, 48) = 21.30$, $p < 0.0001$], with the difference reaching significance in the 6- and 9-month-old mice groups ($p = 0.0183$ and $p = 0.0009$, respectively) (Fig. 5B). Older mice covered larger distances in the central part of the arena [$F(2, 48) = 7.009$, $p = 0.0021$] and this effect reached significance only in the 9-month-old vehicle-treated mice compared with the 3-month-old vehicle-treated counterparts ($p = 0.0044$) (Fig. 5B). Drug treatment also reduced the distance travelled in the peripheral part of the arena [$F(1, 49) = 7.096$, $p = 0.0104$]; however, the effect was not significant in any age group (Fig. 5C). Exposure to CBD:THC reduced the distance covered in the peripheral part of the OF at 3 months of age ($p = 0.0354$).

Exposure to CBD:THC was associated with an increase in total resting time in the OF test compared with the vehicle-treated animals [$F(1, 50) = 25.11$, $p < 0.0001$] (Fig. 5D). This effect was significant in 3-, 6-, and 9-month-old mice ($p = 0.0156$, $p = 0.0004$, $p = 0.0170$, respectively). The main factor age had a significant effect on resting time in the central arena [$F(2, 46) = 5.687$, $p = 0.0062$], and 6-month-old drug-treated mice rested more in the central part than their 3-month-old counterparts ($p = 0.0025$) (Fig. 5E). Multiple comparison test revealed a significant drug-induced increase in resting time in the central part of the arena in 6-month-old mice ($p = 0.0252$).

CBD:THC treatment increased the resting time of the mice in the periphery of the arena [$F(1, 50) = 18.41$, $p < 0.0001$], with a significant effect observed in the 3- ($p = 0.0168$), 6- ($p = 0.0115$), and 9-month-old mice ($p = 0.0225$) (Fig. 5F). Increasing age, on the other hand, reduced the resting time in the periphery [$F(2, 50) = 9.063$, $p = 0.0004$];

Drug treatment decreased the mean speed of movement in the OF arena [$F(1, 48) = 20.65$; $p < 0.0001$] (Fig. 5G). This CBD:THC-induced decrease in total speed was evident in the 3-, 6-, and 9-month-old mice ($p = 0.0127$, $p = 0.0204$, and $p = 0.0061$, respectively). The analysis of the mean speed in the central section of the arena (Fig. 5H) revealed significant effects of both, the treatment [$F(1, 49) = 6.153$;

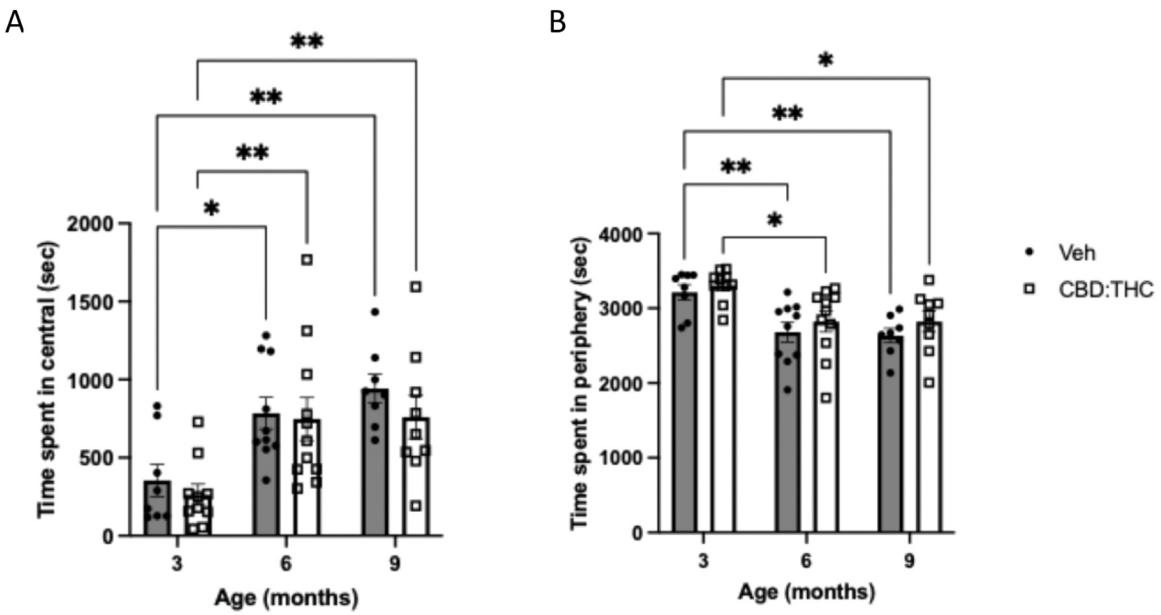

Fig. 4. Time spent in the central (A) and peripheral (B) sections of the OF arena by 5xFAD mice exposed to subcutaneous administration of vehicle or CBD:THC (99:1) 50 mg/kg, for 28 days, measured 2 h after the administration. There were no significant effects due to treatment but there was a significant effect due to the age, with increases in time spent in the central section and decreased time spent in the peripheral section of the OF arena. N = 8–11 per group and treatment. Data presented are individual values for each mouse, and the error bars show mean ± SEM. Two-way ANOVA followed by Sidak's post-hoc test. *p < 0.05, **p < 0.01.

p = 0.0166] and the age (F(2, 49)= 19.09; p < 0.0001], but not as a result of the interaction between the two factors [F(2, 49)= 0.3559; p = 0.7024]. Mean speed in the peripheral part of the arena was significantly reduced by the drug treatment [F(1, 48)= 18.53, p < 0.0001], with this effect being significant in the 3- and 9-month-old mice (p = 0.0192 and p = 0.0043) with a trend toward significance in the 6-month-old group (p = 0.0522) (Fig. 5I).

3.2. Amyloid biology

We next quantified the amount of soluble $A\beta_{1-42}$ by ELISA (Fig. 6A). As expected, amyloid levels increased with age [F(2, 32)= 25.65; p < 0.0001], being higher in 6- (p = 0.0005) and 9-month-old mice (p < 0.0001) compared with 3-month-old mice in the vehicle-treated group, as well as between 6- and 9-month-old mice (p = 0.0450). CBD:THC-treated mice exhibited increased levels of $A\beta_{1-42}$ at 9-month-old as compared with 3-month-old mice (p = 0.0057) (Fig. 6A). No changes associated with the treatment were found [F(1, 32)= 2.280; p = 0.1409], nor in the interaction between factors [F(2, 32)= 2.470, p = 0.1006].

Cortical APP levels were measured by western blot (Fig. 6B). Treatment had no significant effect on APP levels [F(1,40)= 0.0020; p = 0.9643], neither did the interaction between age and treatment [F (2, 40) = 1.600; p = 0.2145]. However, there was an effect associated with age [F(2, 40)= 5.737; p = 0.0064], that was significant at 6 months compared with 3-month-old mice in the vehicle group (p = 0.0444).

3.3. In vivo multiphoton microscopy

We performed an *in vivo* time-course analysis of the progression of amyloid plaques in 6-month-old mice exposed to vehicle or CBD:THC (Fig. 7A and B). Plaques increased their volume during the 28 days observation period [F (1.573, 11.01)= 5.279; p = 0.0303] and the treatment with the cannabinoid mixture did not modify plaque volume [F(1, 7)= 0.2489; p = 0.6332] (Fig. 7C). Plaque complexity was significantly decreased by the treatment with CBD:THC [F(1, 33)= 12.66; p = 0.0012] but did not change with time [F(4, 33)= 0.6301; p = 0.6445] (Fig. 7D). Post test analysis revealed a significant decrease in plaque complexity on day 14th of treatment (p = 0.0038). The amount of methoxy-X04 bound to a plaque was estimated by the plaque total brightness intensity (Fig. 7E). We found a significant effect of the treatment with CBD:THC on plaque intensity [F(1, 35)= 30.22; p < 0.0001], and the multiple comparison test revealed significant reductions on days 14 (p = 0.0067), 21 (p = 0.0012), and 28 (p = 0.0002). There were no changes associated to the time-course [F(4, 35)= 1.366, p = 0.2655]. Plaque density was determined as the ratio between total fluorescence intensity and plaque volume (Fig. 7F) and its quantification revealed a significant effect of the CBD:THC treatment [F (1, 7)= 6.979; p = 0.0333], with significant decreases on days 14 (p = 0.0319), 21 (p = 0.0393), and 28 (p = 0.0481). There were no significant changes associated with treatment duration [F(2.070, 14.49)= 0.2462; p = 0.7921].

Taken together, *in vivo* multiphoton microscopy data point to a CBD:THC-induced increase in plaque homogeneity (protein distribution) in the brain cortex of 5xFAD mice (Fig. 7G).

3.4. In vivo phagocytosis: flow cytometry

A gating strategy scheme was performed to select methoxy-positive microglia (Fig. 8A). After treatment with a 50 mg/kg dose of the CBD:THC mixture, we found no changes in the total percentage of methoxy positive microglial cells in the brain cell suspensions detected by flow cytometry, suggesting a lack of effect of the treatment on phagocytic microglia (Fig. 8B; p = 0.7117). However, methoxy-positive microglia from CBD:THC-treated mice exhibited an increased mean fluorescent intensity (MFI; p = 0.0089), indicative of an increased phagocytic activity by these cells in the treated group (Fig. 8C).

3.5. Protein markers of neuroinflammation

Treatment with CBD:THC did not induce global significant changes in IL1β expression levels in the brain [F(1, 43)= 0.4329; p = 0.5141] (Fig. 9A). There were significant age-dependent effects [F(2, 43)= 3735; p = 0.0319], such that vehicle-treated 6-month-old mice had significantly lower levels than their 3-month-old counterparts (p = 0.0193), and 9-month-old mice exhibited increased levels over 6-month-old mice

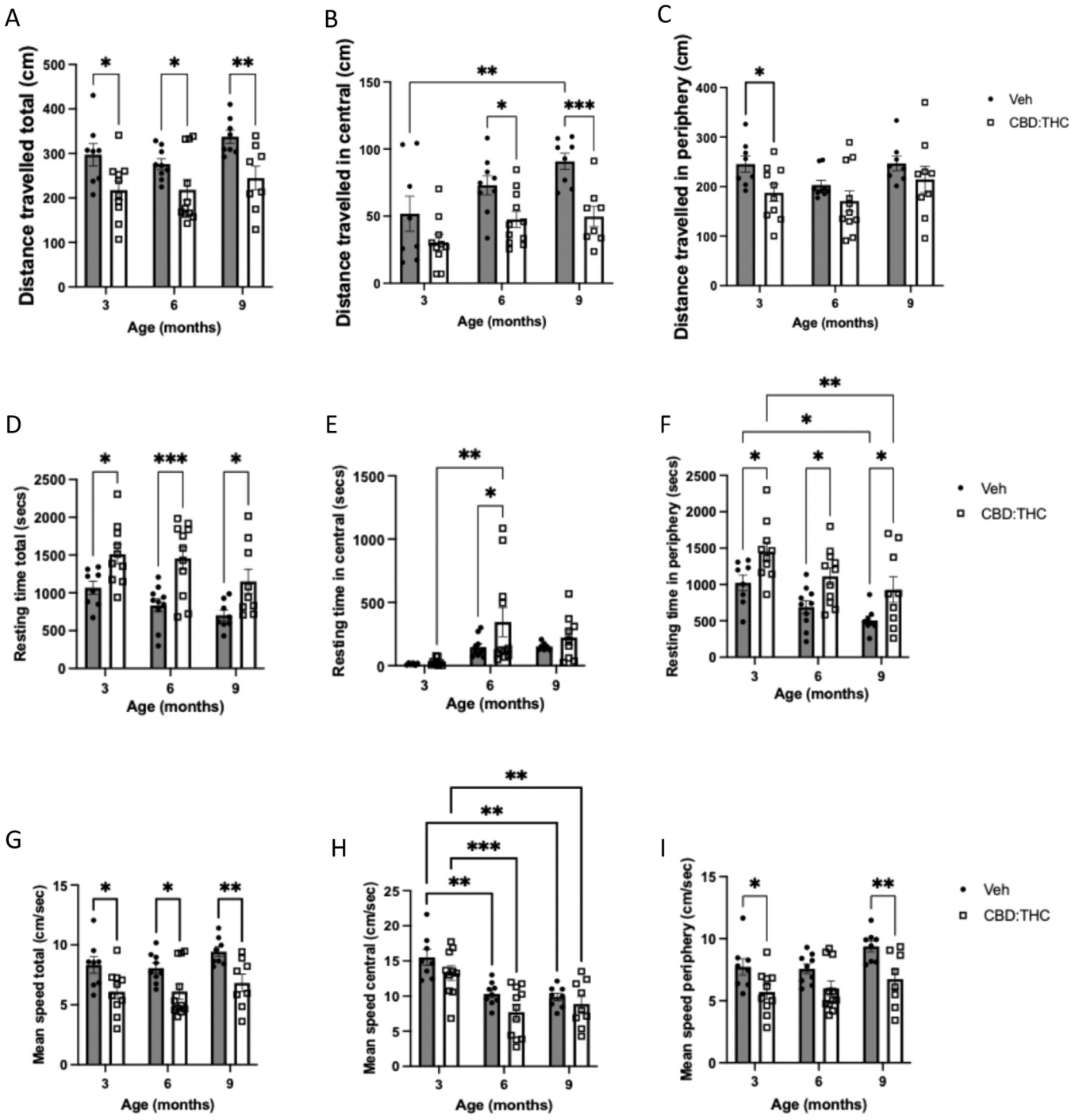

Fig. 5. Locomotor activity of 5xFAD mice exposed to subcutaneous administration of vehicle or CBD:THC (99:1) 50 mg/kg, for 28 days, measured in the OF. Data obtained included total distance travelled in the arena (A), distance covered by the mice in the central part (B), and in the periphery (C), total resting time (D), or in the central (E) and peripheral (F) parts of the arena, and overall mean speed (G), or in the central (H) and peripheral (I) sections of the arena. (A) The total distance covered by mice treated with the mixture of cannabinoids was significantly lower at all ages tested. (B) In the central part of the OF arena, drug effects were found in 6- and 9-month-old mice, while only 3-month-old mice exhibited drug-related changes in the distance covered in the peripheral part (C). Regarding resting time, exposure to CBD:THC led to significant increases in total time at all ages tested (D), an effect that was evident in the central part only in 6-month-old mice (E), and that was mostly due to the increase of resting time spent in the peripheral section of the arena (F). Mean speed was also affected by the treatment with CBD:THC, inducing significant decreases at all ages in total mean speed (G) that was mainly due to changes in mean speed in the peripheral part of the arena (H and I). N = 8–11 per group and treatment. Data presented are mean ± SEM. Two-way ANOVA followed by Sidak's post-hoc test; *p < 0.05, **p < 0.01, ***p < 0.001.

in the CBD:THC group ($p = 0.0476$).

With respect to TREM-2 levels (Fig. 9B), no significant changes were detected due to the treatment [$F(1, 42) = 0.2987$, $p = 0.5876$]. There was a significant effect of age [$F(2, 42) = 6.027$; $p = 0.0050$]; however, the significant difference was confined to the vehicle group, where 9-month-old mice had significantly higher TREM-2 levels than their 3-month-old counterparts ($p = 0.0230$).

CD40 levels (Fig. 9C) were not significantly affected by CBD:THC treatment [$F(1, 43) = 0.2232$, $p = 0.6390$]. There was a significant effect of age [$F(2, 43) = 19.87$; $p < 0.0001$). CD40 levels diminished

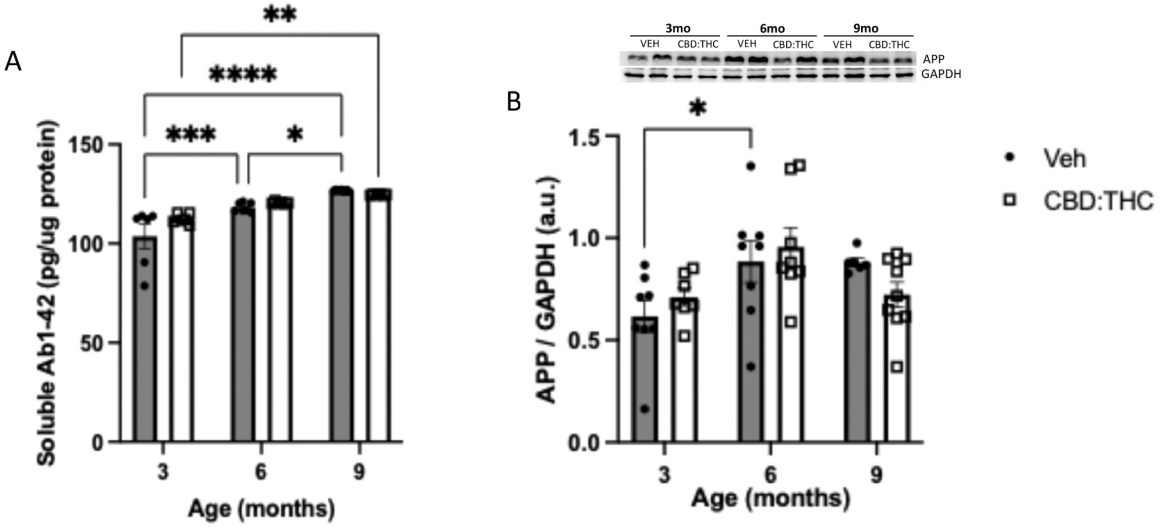

Fig. 6. Hippocampal $A\beta_{1-42}$ and cortical APP levels in 3, 6, and 9 month old mice treated with vehicle or CBD:THC. (A) Protein levels measured by ELISA showed an increase of $A\beta_{1-42}$ due to age at 6 and 9 months of age; treatment with CBD:THC induced a significant increase in soluble levels only at 3 months of age. N = 6–7 per group. (B) Representative western-blot and protein levels of APP; no drug-induced changes were observed, while a significant increase was found in 6-month-old mice when compared with 3-month-old mice treated with vehicle. N = 7–9 per group. Data presented are mean ± SEM. Two-way ANOVA followed by Sidak's post-hoc test; *p < 0.05, **p < 0.01, ***p < 0.001, ****p < 0.0001.

(p = 0.0007) at 6 months of age as compared with 3 months in the vehicle-treated group and then returned to levels observed at 3 months at 9 months of age. CBD:THC-treated mice had significantly higher levels of CD40 protein at 9 months than at 3 and 6 months of age (p < 0.0001).

Finally, no significant changes were found regarding COX-2 protein levels (Fig. 9D) as a function of age [F(2, 43)= 1.719; p = 0.1913] or treatment [F(1, 43)= 0.1312; p = 0.7189].

4. Discussion

The main finding of the present study is that a 28-day treatment with CBD:THC (50 mg/kg) induces a significant alteration of amyloid plaque features in the 5xFAD mouse model of AD. Specifically, the *in vivo* analysis of amyloid plaques in CBD:THC-treated 5xFAD mice reveals significant decreases in fluorescent intensity after staining with methoxy-X04, accompanied by a decrease in plaque protein density. These data suggest that the treatment with CBD:THC modifies the structural features of these pathological structures by turning them into more homogeneous and less dense aggregates (see representative cartoon in Fig. 6).

Amyloid plaque texture, including volume, density, and morphological complexity, plays a pivotal role in determining both the pathogenic trajectory and microglial response in animal models of AD [20]. Multiphoton microscopy reveals that plaque volume strongly influences microglial aggregation and activation so that larger plaques recruit higher numbers of microglia, which also display increased soma volume and reduced process ramification [29]. These microglia undergo dynamic changes, including the polarized extension of processes toward plaque surfaces and sustained phagocytic activity at the plaque-glia interface, a phenomenon most pronounced in dense-core plaques [29]. Importantly, plaque density shapes the efficacy of microglial containment and clearance; highly fibrillar and compact plaques tend to be surrounded by a more stable, less migratory microglial population. Plaques with higher morphological complexity, characterized by irregular boundaries and heterogeneous composition, impacting not only microglial morphology but also local tissue architecture, further amplifying synaptic dysfunction and cognitive decline [29,56]. Finally, longitudinal imaging studies further indicate that plaque growth is determined by the inverse correspondence between microglial coverage and plaque structure: regions with lower microglial reactivity manifest greater plaque expansion, while high microglial volume correlates with plaque shrinkage or stabilization [8,9,29]. This dynamic bidirectional relationship underscores the biological importance of textural plaque features for the balance between neurotoxicity and immune-mediated containment.

The molecular basis for the changes reported herein may reside on a direct effect of CBD and/or THC on the amyloid fibrillation process or on the activation of cannabinoid receptors located on neighboring cells. In the first case, previous reports confirmed that THC is able to prevent amyloid aggregation *in vitro* [24] and to disrupt fibrils stability [36]. Also, Chrobak et al. [17] have reported on the ability of CBD to physically interact with $A\beta_{25-35}$ peptide, thus decreasing its aggregation and toxicity by altering its structure [17]. These observations could partially explain the changes here reported on the structural features of amyloid plaques in the cortex of 5xFAD mice.

On the other hand, we and others have recently reported that the activation of microglial cannabinoid CB_2 receptors modifies amyloid dynamics in the 5xFAD mouse model of AD [58,60]. Furthermore, it was recently shown that the expression of microglial CB_2 receptors triggers an inflammatory phenotype in these cells, being a potent immunomodulator in the brain [47]. It must be mentioned, however, that the role of CB_2 receptors in AD is still controversial and that their contribution has been reported to be of limited relevance in the AβPP/PS1 mouse model of AD [6].

Our data also reveal the effect of the CBD:THC mixture on the microglial ability to phagocytose amyloid beta peptides. Microglial cells isolated from CBD:THC-treated mice contained significantly elevated amounts of methoxy-X04, suggesting an increased phagocytic activity of these cells in the treated group. To the best of our knowledge, this is the first *in vivo* observation of a facilitatory effect of these cannabinoids on the phagocytic properties of adult, activated microglia. Our data confirm the stimulatory effect of CBD on microglial phagocytosis *in vitro* previously reported [30,75]. These authors found that CBD (5–10 μM) enhanced microglial phagocytosis of synthetic amyloid fibrils or microbeads in primary cultures of neonatal microglia as well as in BV2 cells, in a process mediated by the interaction of CBD with TRPV2, but not TRPV1 or TRPV4. On the contrary, Aguiar et al. [2] have recently reported the absence of effects of CBD (3 mg/kg) on microglial phagocytic activity in hippocampi from healthy rats [2].

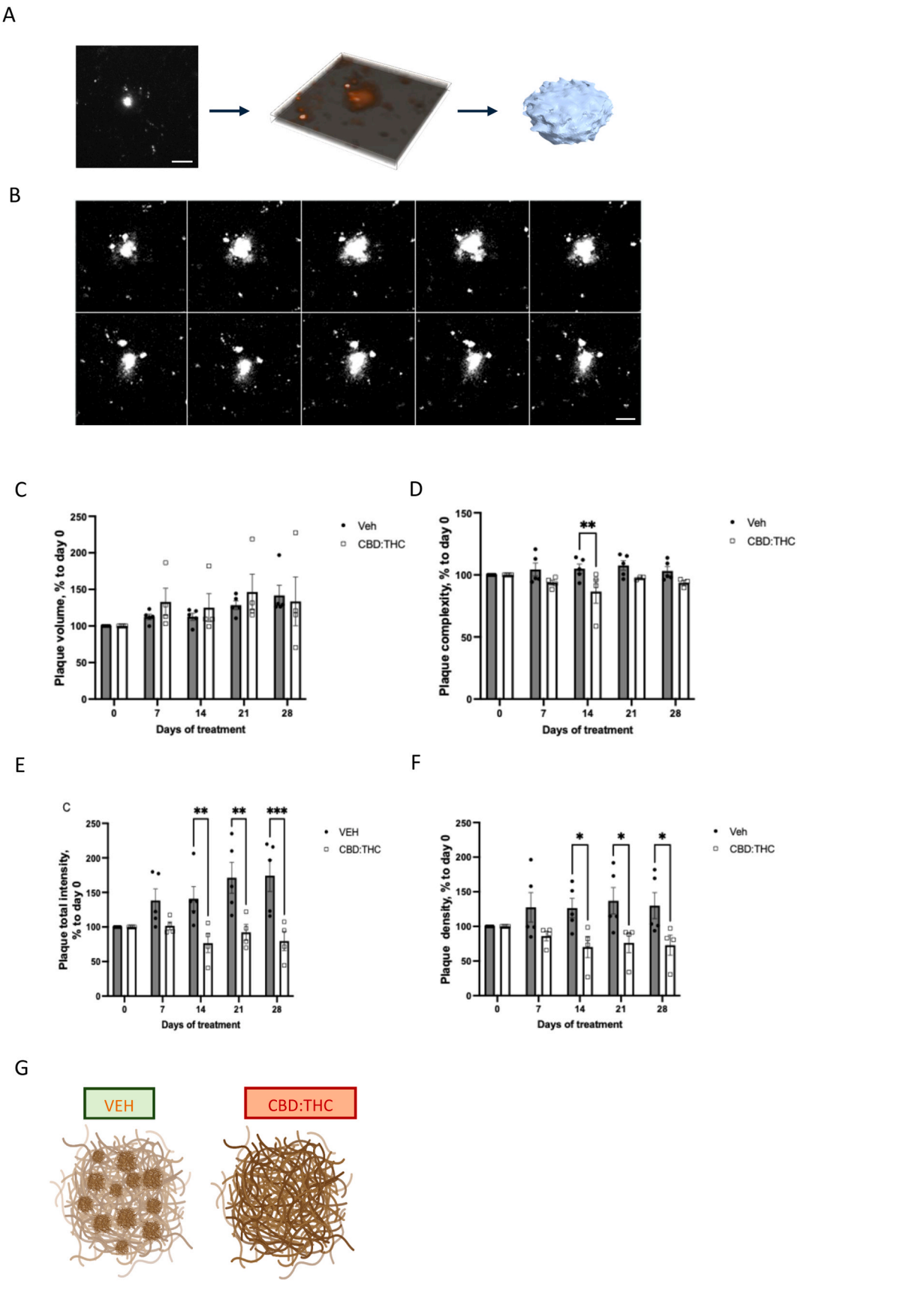

(caption on next page)

Fig. 7. Time-course of amyloid plaque evolution in the cortex of 5xFAD mice exposed to vehicle or CBD:THC for 28 days, by *in vivo* multiphoton microscopy. (A) Image processing of amyloid plaques labelled with methoxy-X04 (10 mg/kg), administered i.p. 24 h prior to each imaging session. Z-projection of a stack of images obtained from one single plaque (left), and subsequent three-dimensional representation (center), and final reconstruction of its structural features (right). (B) Representative Z-projection of a stack of images obtained over a 28-day period (one per week) in mice treated with vehicle (upper panel) or CBD:THC (lower panel). The time-course of the structural features of cortical amyloid plaques in the mouse brain included volume (C), complexity (D), total intensity (E) and density (F). (C) Plaque volume increased during the 28-days of imaging. No changes were associated to the exposure to cannabinoids. (D) Amyloid plaques exhibited a lower structural complexity in mice treated with CBD:THC. (E) Fluorescence intensity of amyloid plaques increased with time and this increase was prevented by the exposure CBD:THC, as evident on days 14, 21, and 28. (F) Plaque protein density was increased with time but treatment with the cannabinoid mixture prevented this increase. This effect was evident on days 14, 21, and 28. (G) Cartoon showing a graphic representation of plaque appearance after exposure to CBD:THC. N = 4 in the CBD:THC treatment group and N = 5 in the vehicle-treated group. Data presented are mean ± SEM. Two-way ANOVA followed by Sidak's post-hoc test; *$p < 0.05$, **$p < 0.01$, ***$p < 0.001$. Scale bars: 10 μm.

By modulating microglial phagocytic activity, CBD:THC may contribute to amyloid plaque dynamics. It is currently accepted that microglial cells play a crucial role in the development, growth, and maintenance of neuritic plaques [67], although conflicting views exist at the present time [12,76]. Some authors have suggested that microglia are responsible for the efficient removal of amyloid-enriched deposits, while others have shown that they may be the main source of newly-formed plaques, playing a role in their seeding process [67]. As THC and CBD have been shown to be significant modulators of microglial activity [19,45], we may speculate that they may also participate in amyloid-related microglial function, thus contributing to the compaction of neuritic plaques, as suggested by our present data.

These changes were not accompanied by significant alterations in behavior or in the inflammation-related molecular components analyzed (IL-1β, TREM2, or COX-2). Though we tested several ages (3, 6, and 9 months) and, subsequently, different stages of disease progression (early, established, and advanced, respectively), modest modifications were observed. A potential explanation for this mismatch could be the lack of correspondence that is known to occur among amyloid deposition and some of the key phenotypic features of AD with a closer relationship between tau deposits and, for instance, memory loss [4].

The behavioral changes that are characteristic of 5xFAD mice have been well studied [27,51]. 5xFAD mice exhibit increased locomotion, depression and anxiety, and these changes are more pronounced in females than in males. Some inconsistencies have been observed in the literature, but the reasons for this remain unknown. Importantly, a recent study by Sasmita et al. [65] has unveiled the previously unknown variability dependent on the germ line through which the AD transgene is inherited in 5xFAD transgenic mice [65]. In our case, this potential variability was prevented, as the transgene was inherited paternally only.

It is important to note that recent studies have underscored the neuroprotective properties of CBD, revealing its ability to simultaneously modulate memory enhancement, neuroinflammatory processes, and pathological protein dynamics [28,57,69]. Chronic oral administration of CBD to aged SAMP8 mice led to improvements in object and spatial memory, as reflected in tasks such as novel object recognition and the Morris water maze, with higher doses required for restoring long-term memory deficits. These cognitive benefits were accompanied by reductions in neuroinflammatory markers such as astrocytosis in hippocampus and microgliosis in medial prefrontal cortex, as well as microglial polarization toward a neuroprotective M2 phenotype in 5xFAD mice. At the molecular level, CBD reduced the aggregation of amyloid and hyperphosphorylated tau, counteracted protein axonal transport between neurons, decreased oxidative stress, and restored neuronal plasticity in cortical and hippocampal cultures. Taken together, these recent data highlight the potential of CBD as a novel approach to tackle some of the molecular and behavioral features of AD [10,46].

The data presented herein show modest behavioral effects following chronic dosing with CBD:THC, including decreased locomotion. We acknowledge that the absence of a WT mice group is a limitation of this study and impedes a complete characterization of the phenotypic changes observed. CBD:THC treatment significantly affected locomotion as it reduced distance travelled, increased resting time, and decreased speed in the OF arena (in both central and peripheral sections). There were no remarkable drug effects on any other measured behavioral endpoints, although subtle age-dependent effects on anxiety- and depression-like behaviors were also shown, in agreement with previous studies [5,33]. Cannabinoid-induced inhibition of motor activity has been long recognized, with the dose of the specific cannabinoids representing a crucial factor to consider [62]. Overall, our present data suggest a limited impact of the chronic exposure to CBD:THC on behavior features of 5xFAD mice.

Current pharmacological treatment of AD is based on two main types of drugs: acetylcholinesterase inhibitors (AChEIs, such as donepezil or rivastigmine) and antagonists of glutamatergic receptors (i.e. memantine), that have limited influence on these behavioral features [35]. Regarding motor activity, their net effect depends on individual susceptibility, disease stage, and drug tolerability; AChEIs may help reduce agitated or aberrant motor activity in AD, especially in advanced cases, but can also cause movement disorders in a minority of patients [59]. Memantine has little direct effect on motor activity, with side effects more commonly related to dizziness or confusion. Also, AChEIs can alleviate anxiety in AD patients but they may also provoke it as a side effect, while memantine shows more consistent anxiolytic benefits. Finally, these drugs show limited efficacy regarding depression [22,32,38].

In summary, *in vivo* exposure to 50 mg/kg of a CBD:THC (99:1) mixture, s.c., for 28 consecutive days, enhanced *in vivo* microglial phagocytic activity of beta amyloid, leading to significant changes in neuritic plaque features (as revealed by multiphoton microscopy). In addition, limited behavioral effects were associated with the treatment with the CBD:THC mixture.

Author's contributions

SRME treated mice and performed behavioral and multiphoton experiments; MTG made molecular biology and flow cytometry determinations; AMMR made molecular biology studies; DHA wrote the software for plaque analysis; RM designed and built the multiphoton microscope; CJH provided materials; WHH contributed to the design of the study and authoring of the manuscript; JR designed and supervised the experiments and wrote the manuscript. All authors read and agreed on the final version of this manuscript.

CRediT authorship contribution statement

Samuel Ruiz de Martín Esteban: Writing – review & editing, Writing – original draft, Methodology, Investigation, Data curation. **Cecilia Hillard:** Writing – review & editing, Resources, Investigation, Formal analysis. **Ricardo Mostany:** Writing – review & editing, Software, Resources, Investigation, Data curation. **Julián Romero:** Writing – review & editing, Writing – original draft, Supervision, Project administration, Methodology, Investigation, Funding acquisition, Conceptualization. **William Hind:** Writing – review & editing, Validation, Resources, Funding acquisition, Formal analysis, Conceptualization. **Ana Maria Martínez-Relimpio:** Writing – review & editing,

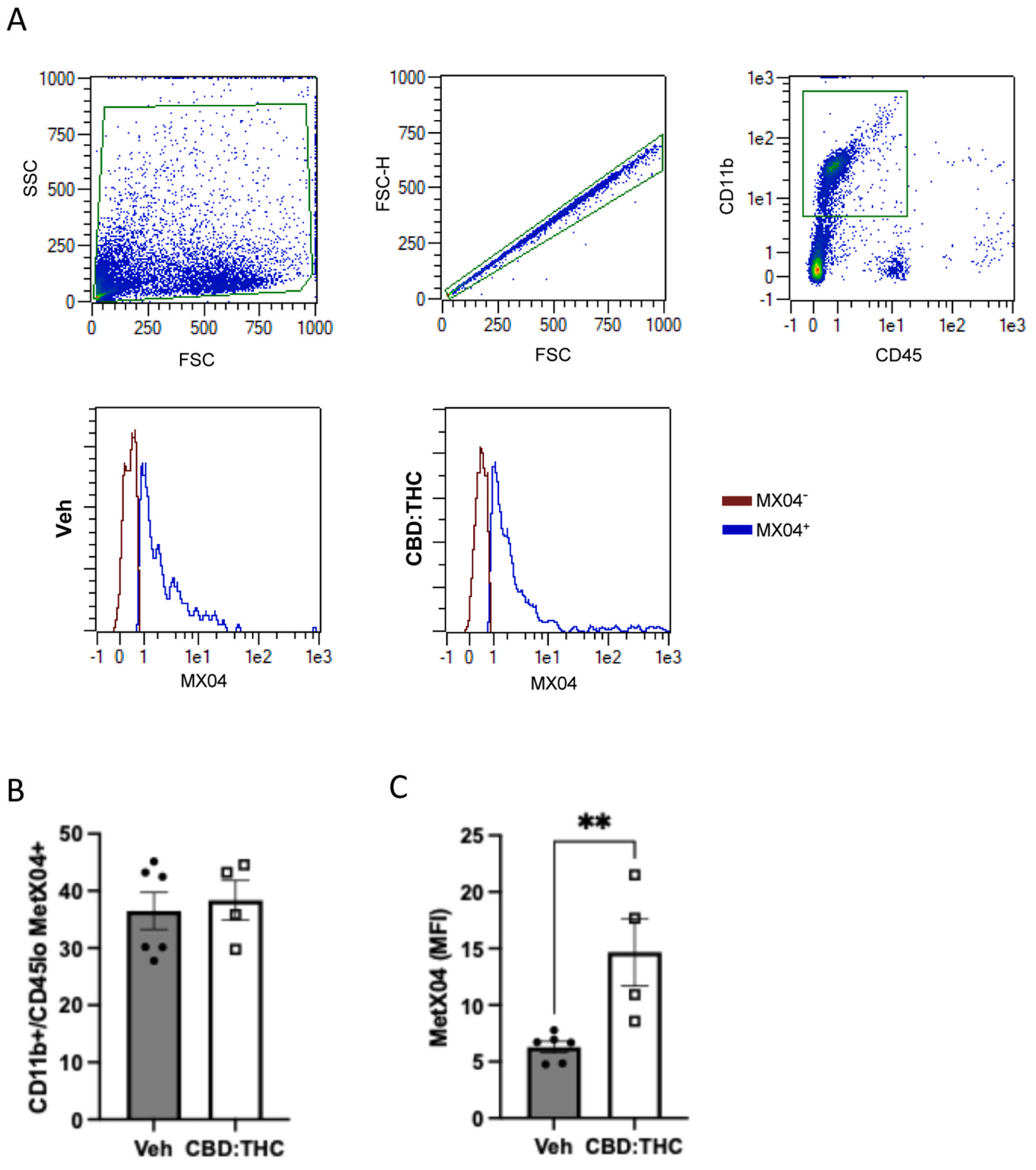

Fig. 8. Flow cytometry data on total number of microglial cells and their phagocytic activity. (A) Gating strategy to identify CD11b+ CD45lo X04 + microglia, from left to right; cells, singlets, and microglia, and representative histogram showing the methoxy-X04 signal intensity of Aβ phagocytic microglia (MX04 + microglia) and non-Aβ phagocytic microglia (MX04 − microglia). While the total number of microglial cells was not affected by the treatment (B), their phagocytic activity was significantly increased **(C)**. N = 4–6 mice per group. Data are presented as mean ± SEM. Unpaired-*t*-test. **p < 0.01.

Investigation, Data curation. **Maria Teresa Grande:** Writing – review & editing, Writing – original draft, Supervision, Project administration, Methodology, Investigation, Conceptualization. **Diego Herráez-Aguilar:** Writing – review & editing, Validation, Software, Methodology, Investigation.

Funding

Funded by Jazz Pharmaceuticals Research UK Ltd and by Ministerio de Ciencia e Innovación – Agencia Estatal de Investigación and Fondo Europeo de Desarrollo Regional (Proyecto PID2022–138461OB-I00,

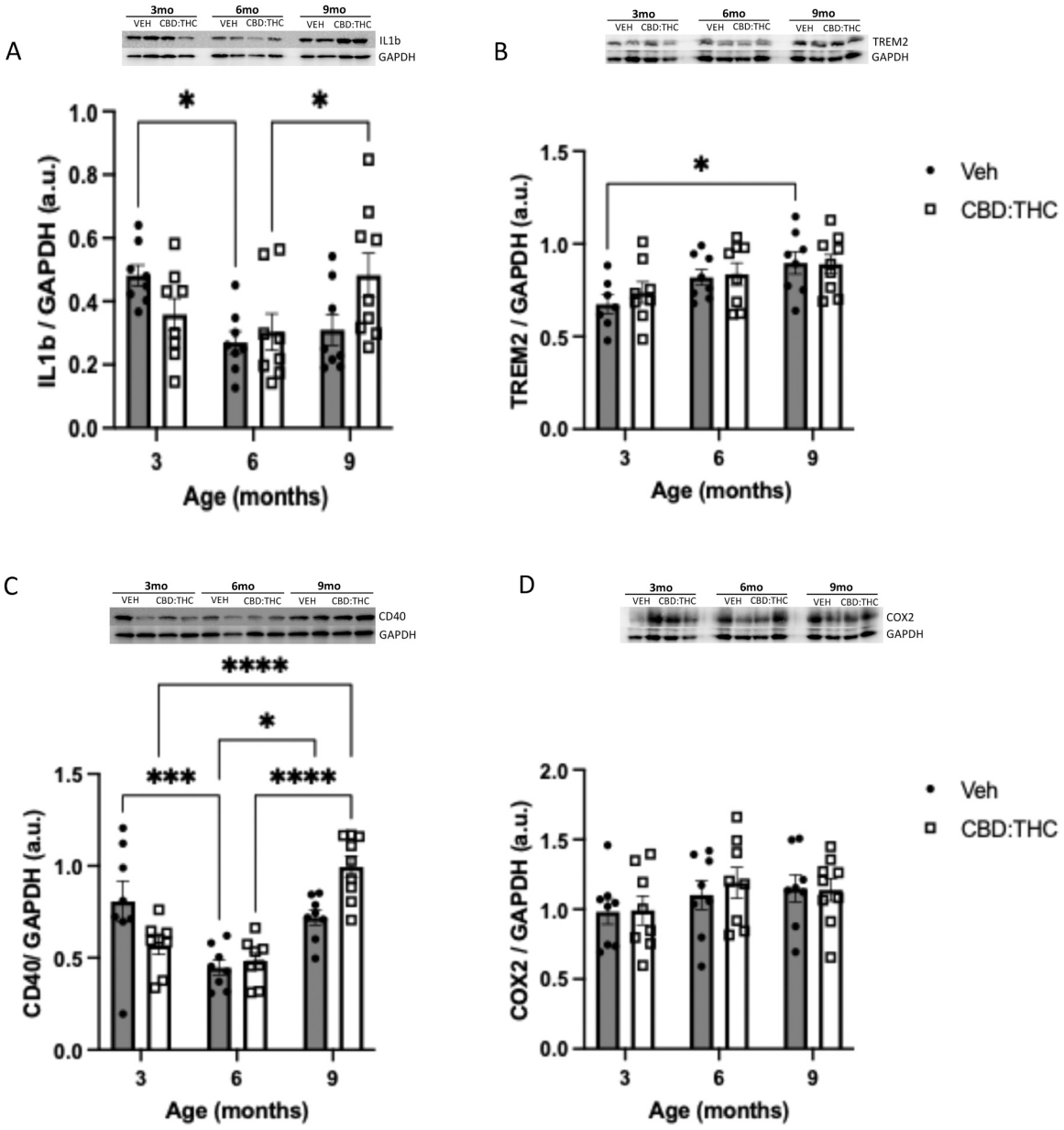

Fig. 9. Protein markers of neuroinflammation measured by western blot. (A) IL1β levels varied with age in the vehicle (6 months) and in CBD:THC (9 months) groups; exposure to CBD:THC increased IL1β levels in 9-month-old mice. (B) Protein levels of the microglial marker TREM2 were elevated as a function of age, while no changes were associated to the treatment. (C) CD40 levels exhibited a "u-shaped" pattern with age and followed opposite patterns after treatment with CBD:THC at 3 (decrease) and 9 (increase) months of age. (D) COX-2 levels were not modified by age or treatment. N = 8–9 per group and treatment. Data presented as individual values; error bars show mean ± SEM. Two-way ANOVA followed by Sidak's post-hoc test. *p < 0.05, ***p < 0.001, ****p < 0.0001.

Supported by PID2022-138461OB-I00, MICIU/AEI /10.13039/501100011033 and by FEDER, UE). Jazz Pharmaceuticals supervised the study design and participated in data analysis, and in the decision to submit this manuscript.

Declaration of Competing Interest

- SRME, MTG, AMMR, DHA, RM, and JR declare that they have no conflicts of interest.
- WHH is an employee of Jazz Pharmaceuticals Research Ltd, where he receives salary and holds shares.
- CJH is a member of the Board of Scientific Directors and has equity in Formulate Biosciences, Inc.

Appendix A. Supporting information

Supplementary data associated with this article can be found in the online version at doi:10.1016/j.biopha.2025.118902.

Data availability

Data will be made available on request.

References

[1] G. Abate, D. Uberti, S. Tambaro, Potential and limits of cannabinoids in Alzheimer's disease therapy, Biology 10 (2021), https://doi.org/10.3390/biology10060542.
[2] A.F.L. Aguiar, R.M.P. Campos, A.R. Isaac, Y. Paes-Colli, V.M. Carvalho, L. S. Sampaio, et al., Long-term treatment with cannabidiol-enriched cannabis extract

induces synaptic changes in the adolescent rat hippocampus, Int. J. Mol. Sci. 24 (2023), https://doi.org/10.3390/ijms241411775.
[3] N. Aparicio, M.T. Grande, S. Ruiz de Martín Esteban, A. López, G. Ruiz-Pérez, M. Amores, et al., Role of interleukin 1-beta in the inflammatory response in a fatty acid amide hydrolase-knockout mouse model of Alzheimer's disease, Biochem. Pharm. 157 (2018) 202–209, https://doi.org/10.1016/j.bcp.2018.09.009.
[4] A. Ardura-Fabregat, E.W.G.M. Boddeke, A. Boza-Serrano, S. Brioschi, S. Castro-Gomez, K. Ceyzériat, et al., Targeting neuroinflammation to treat Alzheimer's disease, CNS Drugs 31 (2017) 1057–1082, https://doi.org/10.1007/s40263-017-0483-3.
[5] M.A. Arnanz, S. Ruiz de Martín Esteban, A.M. Martínez Relimpio, N. Rimmerman, N. Tweezer Zaks, M.T. Grande, et al., Effects of chronic, low-dose cannabinoids, cannabidiol, delta-9-tetrahydrocannabinol and a combination of both, on amyloid pathology in the 5xFAD mouse model of Alzheimer's disease, Cannabis cannabinoid Res (2023), https://doi.org/10.1089/can.2023.0101.
[6] E. Aso, P. Andrés-Benito, M. Carmona, R. Maldonado, I. Ferrer, Cannabinoid receptor 2 participates in amyloid-β processing in a mouse model of Alzheimer's disease but plays a minor role in the therapeutic properties of a cannabis-based medicine, J. Alzheimer'S. Dis. 51 (2016) 489–500, https://doi.org/10.3233/JAD-150913.
[7] E. Aso, A. Sánchez-Pla, E. Vegas-Lozano, R. Maldonado, I. Ferrer, Cannabis-based medicine reduces multiple pathological processes in AβPP/PS1 mice, J. Alzheimers Dis. 43 (2015) 977–991, https://doi.org/10.3233/JAD-141014.
[8] R. Baron, A.A. Babcock, A. Nemirovsky, B. Finsen, A. Monsonego, Accelerated microglial pathology is associated with Aβ plaques in mouse models of Alzheimer's disease, Aging Cell 13 (2014) 584–595, https://doi.org/10.1111/acel.12210.
[9] T. Bolmont, F. Haiss, D. Eicke, R. Radde, C.A. Mathis, W.E. Klunk, et al., Dynamics of the microglial/amyloid interaction indicate a role in plaque maintenance, J. Neurosci. Off. J. Soc. Neurosci. 28 (2008) 4283–4292, https://doi.org/10.1523/JNEUROSCI.4814-07.2008.
[10] A.J. de L. Bomfim, S.M.F. Zuze, D. Fabrício, M. de, R.M. de P. Pessoa, J.A.S. Crippa, M.H.N. Chagas, Effects of the acute and chronic administration of cannabidiol on cognition in humans and animals: a systematic review, Cannabis cannabinoid Res 8 (2023) 955–973, https://doi.org/10.1089/can.2023.0086.
[11] A. Can, D.T. Dao, C.E. Terrillion, S.C. Piantadosi, S. Bhat, T.D. Gould, The tail suspension test, J. Vis. Exp. (2012) e3769, https://doi.org/10.3791/3769.
[12] B.T. Casali, K.P. MacPherson, E.G. Reed-Geaghan, G.E. Landreth, Microglia depletion rapidly and reversibly alters amyloid pathology by modification of plaque compaction and morphologies, Neurobiol. Dis. 142 (2020) 104956, https://doi.org/10.1016/j.nbd.2020.104956.
[13] M.J. Casarejos, J. Perucho, A. Gomez, M.P. Muñoz, M. Fernandez-Estevez, O. Sagredo, et al., Natural cannabinoids improve dopamine neurotransmission and tau and amyloid pathology in a mouse model of tauopathy, J. Alzheimers Dis. 35 (2013) 525–539, https://doi.org/10.3233/JAD-130050.
[14] R. Chen, J. Zhang, N. Fan, Z. Teng, Y. Wu, H. Yang, et al., Δ9-THC-caused synaptic and memory impairments are mediated through COX-2 signaling, Cell 155 (2013) 1154–1165, https://doi.org/10.1016/j.cell.2013.10.042.
[15] D. Cheng, A.S. Spiro, A.M. Jenner, B. Garner, T. Karl, Long-term cannabidiol treatment prevents the development of social recognition memory deficits in Alzheimer's disease transgenic mice, J. Alzheimers Dis. 42 (2014) 1383–1396, https://doi.org/10.3233/JAD-140921.
[16] R. Chesworth, D. Cheng, C. Staub, T. Karl, Effect of long-term cannabidiol on learning and anxiety in a female Alzheimer's disease mouse model, Front. Pharm. 13 (2022) 931384, https://doi.org/10.3389/fphar.2022.931384.
[17] W. Chrobak, D.W. Pacut, F. Blomgren, A. Rodin, J. Swenson, I. Ermilova, Component of cannabis, cannabidiol, as a possible drug against the cytotoxicity of Aβ(31-35) and Aβ(25-35) peptides: an investigation by molecular dynamics and well-tempered metadynamics simulations, ACS Chem. Neurosci. 12 (2021) 660–674, https://doi.org/10.1021/acschemneuro.0c00692.
[18] M. Coles, G.Z. Steiner-Lim, T. Karl, Therapeutic properties of multi-cannabinoid treatment strategies for Alzheimer's disease, Front. Neurosci. 16 (2022) 962922, https://doi.org/10.3389/fnins.2022.962922.
[19] L. Cutando, A. Busquets-Garcia, E. Puighermanal, M. Gomis-González, J. M. Delgado-García, A. Gruart, et al., Microglial activation underlies cerebellar deficits produced by repeated cannabis exposure, J. Clin. Invest 123 (2013) 2816–2831, https://doi.org/10.1172/JCI67569.
[20] J. Dong, R. Revilla-Sanchez, S. Moss, P.G. Haydon, Multiphoton in vivo imaging of amyloid in animal models of Alzheimer's disease, Neuropharmacology 59 (2010) 268–275, https://doi.org/10.1016/j.neuropharm.2010.04.007.
[21] A.L. Ducote, R.L. Voglewede, R. Mostany, Dendritic spines of layer 5 pyramidal neurons of the aging somatosensory cortex exhibit reduced volumetric remodeling, J. Neurosci. Off. J. Soc. Neurosci. 44 (2024), https://doi.org/10.1523/JNEUROSCI.1378-24.2024.
[22] R.J. Elsworthy, S. Aldred, Depression in Alzheimer's disease: an alternative role for selective serotonin reuptake inhibitors? J. Alzheimers Dis. 69 (2019) 651–661, https://doi.org/10.3233/JAD-180780.
[23] G. Esposito, C. Scuderi, C. Savani, L.J. Steardo, D. De Filippis, P. Cottone, et al., Cannabidiol in vivo blunts beta-amyloid induced neuroinflammation by suppressing IL-1beta and iNOS expression, Br. J. Pharm. 151 (2007) 1272–1279, https://doi.org/10.1038/sj.bjp.0707337.
[24] L.M. Eubanks, C.J. Rogers, A.E. Beuscher, 4th, G.F. Koob, A.J. Olson, T. J. Dickerson, et al., A molecular link between the active component of marijuana and Alzheimer's disease pathology, Mol. Pharm. 3 (2006) 773–777, https://doi.org/10.1021/mp060066m.
[25] T.J. Flanigan, Y. Xue, S. Kishan Rao, A. Dhanushkodi, M.P. McDonald, Abnormal vibrissa-related behavior and loss of barrel field inhibitory neurons in 5xFAD transgenics, Genes. Brain. Behav. 13 (2014) 488–500, https://doi.org/10.1111/gbb.12133.
[26] E. Fordjour, C.F. Manful, A.A. Sey, R. Javed, T.H. Pham, R. Thomas, et al., Cannabis: a multifaceted plant with endless potentials, Front. Pharm. 14 (2023) 1200269, https://doi.org/10.3389/fphar.2023.1200269.
[27] S. Forner, S. Kawauchi, G. Balderrama-Gutierrez, E.A. Kramár, D.P. Matheos, J. Phan, et al., Systematic phenotyping and characterization of the 5xFAD mouse model of Alzheimer's disease, Sci. Data 8 (2021) 270, https://doi.org/10.1038/s41597-021-01054-y.
[28] M.N. Goodland, S. Banerjee, M.L. Niehoff, B.J. Young, H. Macarthur, A.A. Butler, et al., Cannabidiol improves learning and memory deficits and alleviates anxiety in 12-month-old SAMP8 mice, PLoS One 20 (2025) e0296586, https://doi.org/10.1371/journal.pone.0296586.
[29] M. Gotkiewicz, J. Capra, P.O. Miettinen, T. Natunen, H. Tanila, Three-dimensional view of microglia-amyloid plaque interactions, Glia 73 (2025) 196–209, https://doi.org/10.1002/glia.24628.
[30] S. Hassan, K. Eldeeb, P.J. Millns, A.J. Bennett, S.P.H. Alexander, D.A. Kendall, Cannabidiol enhances microglial phagocytosis via transient receptor potential (TRP) channel activation, Br. J. Pharm. 171 (2014) 2426–2439, https://doi.org/10.1111/bph.12615.
[31] A. Holtmaat, T. Bonhoeffer, D.K. Chow, J. Chuckowree, V. De Paola, S.B. Hofer, et al., Long-term, high-resolution imaging in the mouse neocortex through a chronic cranial window, Nat. Protoc. 4 (2009) 1128–1144, https://doi.org/10.1038/nprot.2009.89.
[32] Y.-Y. Huang, Y.-H. Gan, L. Yang, W. Cheng, J.-T. Yu, Depression in Alzheimer's disease: epidemiology, mechanisms, and treatment, Biol. Psychiatry 95 (2024) 992–1005, https://doi.org/10.1016/j.biopsych.2023.10.008.
[33] L.P. Iglesias, L. Bedeschi, D.C. Aguiar, L. Asth, F.A. Moreira, Effects of Δ(9)-THC and Type-1 cannabinoid receptor agonists in the elevated plus maze test of anxiety: a systematic review and meta-analysis, Cannabis cannabinoid Res 8 (2023) 24–33, https://doi.org/10.1089/can.2022.0078.
[34] E. Janefjord, J.L.V. Mååg, B.S. Harvey, S.D. Smid, Cannabinoid effects on β amyloid fibril and aggregate formation, neuronal and microglial-activated neurotoxicity in vitro, Cell. Mol. Neurobiol. 34 (2014) 31–42, https://doi.org/10.1007/s10571-013-9984-x.
[35] R.W. Jones, A review comparing the safety and tolerability of memantine with the acetylcholinesterase inhibitors, Int. J. Geriatr. Psychiatry 25 (2010) 547–553, https://doi.org/10.1002/gps.2384.
[36] P.K. Kanchi, A.K. Dasmahapatra, Destabilization of the Alzheimer's amyloid-β protofibrils by THC: A molecular dynamics simulation study, J. Mol. Graph. Model 105 (2021) 107889, https://doi.org/10.1016/j.jmgm.2021.107889.
[37] T. Karl, R. Pabst, S. von Hörsten, Behavioral phenotyping of mice in pharmacological and toxicological research, Exp. Toxicol. Pathol. Off. J. Ges. fur Toxikol. Pathol. 55 (2003) 69–83, https://doi.org/10.1078/0940-2993-00301.
[38] T. Kishi, S. Matsunaga, N. Iwata, A meta-analysis of memantine for depression, J. Alzheimers Dis. 57 (2017) 113–121, https://doi.org/10.3233/JAD-161251.
[39] W.E. Klunk, B.J. Bacskai, C.A. Mathis, S.T. Kajdasz, M.E. McLellan, M.P. Frosch, et al., Imaging Abeta plaques in living transgenic mice with multiphoton microscopy and methoxy-X04, a systemically administered Congo red derivative, J. Neuropathol. Exp. Neurol. 61 (2002) 797–805, https://doi.org/10.1093/jnen/61.9.797.
[40] D.S. Knopman, H. Amieva, R.C. Petersen, G. Chételat, D.M. Holtzman, B.T. Hyman, et al., Alzheimer disease, Nat. Rev. Dis. Prim. 7 (2021) 33, https://doi.org/10.1038/s41572-021-00269-y.
[41] M. Komada, K. Takao, T. Miyakawa, Elevated plus maze for mice, J. Vis. Exp. (2008), https://doi.org/10.3791/1088.
[42] A. López, N. Aparicio, M.R. Pazos, M.T. Grande, M.A. Barreda-Manso, I. Benito-Cuesta, et al., Cannabinoid CB2 receptors in the mouse brain: relevance for Alzheimer's disease, J. Neuroinflamm. 15 (2018) 158, https://doi.org/10.1186/s12974-018-1174-9.
[43] L.M. Lueptow, Novel object recognition test for the investigation of learning and memory in mice, J. Vis. Exp. (2017), https://doi.org/10.3791/55718.
[44] M. Maccarrone, V. Di Marzo, J. Gertsch, U. Grether, A.C. Howlett, T. Hua, et al., Goods and Bads of the Endocannabinoid System as a Therapeutic Target: Lessons Learned after 30 Years, Pharmacol. Rev. 75 (2023) 885–958, https://doi.org/10.1124/pharmrev.122.000600.
[45] A.M. Martín-Moreno, D. Reigada, B.G. Ramírez, R. Mechoulam, N. Innamorato, A. Cuadrado, et al., Cannabidiol and other cannabinoids reduce microglial activation in vitro and in vivo: relevance to Alzheimer's disease, Mol. Pharm. 79 (2011) 964–973, https://doi.org/10.1124/mol.111.071290.
[46] J.V. Mello-Hortega, C.S. de Oliveira, V.S. de Araujo, L. Furtado-Alle, L.V. Tureck, R. L.R. Souza, Cannabidiol and Alzheimer disease: a comprehensive review and in silico insights into molecular interactions, Eur. J. Neurosci. 62 (2025) e70229, https://doi.org/10.1111/ejn.70229.
[47] A. Moe, A. Rayasam, G. Sauber, R.K. Shah, A. Doherty, C.-Y. Yuan, et al., Type 2 cannabinoid receptor expression on microglial cells regulates neuroinflammation during graft-versus-host disease, J. Clin. Invest 134 (2024), https://doi.org/10.1172/JCI175205.
[48] R. Mostany, J.E. Anstey, K.L. Crump, B. Maco, G. Knott, C. Portera-Cailliau, Altered synaptic dynamics during normal brain aging, J. Neurosci. Off. J. Soc. Neurosci. 33 (2013) 4094–4104, https://doi.org/10.1523/JNEUROSCI.4825-12.2013.
[49] G.M. Nielson, Dual marching cubes, IEEE Vis. 2004 (2004) 489–496, https://doi.org/10.1109/VISUAL.2004.28.
[50] H. Oakley, S.L. Cole, S. Logan, E. Maus, P. Shao, J. Craft, et al., Intraneuronal beta-amyloid aggregates, neurodegeneration, and neuron loss in transgenic mice with five familial Alzheimer's disease mutations: potential factors in amyloid plaque

formation, J. Neurosci. 26 (2006) 10129–10140, https://doi.org/10.1523/JNEUROSCI.1202-06.2006.
[51] A.L. Oblak, P.B. Lin, K.P. Kotredes, R.S. Pandey, D. Garceau, H.M. Williams, et al., Comprehensive evaluation of the 5XFAD mouse model for preclinical testing applications: a MODEL-AD study, Front. Aging Neurosci. 13 (2021) 713726, https://doi.org/10.3389/fnagi.2021.713726.
[52] N. Otsu, A threshold selection method from gray-level histograms, IEEE Trans. Syst. Man. Cyber 9 (1979) 62–66, https://doi.org/10.1109/TSMC.1979.4310076.
[53] P. Pacher, N.M. Kogan, R. Mechoulam, Beyond THC and endocannabinoids, Annu. Rev. Pharmacol. Toxicol. 60 (2020) 637–659, https://doi.org/10.1146/annurev-pharmtox-010818-021441.
[54] P.H. Patra, E. Serafeimidou-Pouliou, M. Bazelot, B.J. Whalley, C.M. Williams, A. J. McNeish, Cannabidiol improves survival and behavioural co-morbidities of Dravet syndrome in mice, Br. J. Pharm. 177 (2020) 2779–2792, https://doi.org/10.1111/bph.15003.
[55] T.A. Pologruto, B.L. Sabatini, K. Svoboda, ScanImage: flexible software for operating laser scanning microscopes, Biomed. Eng. Online 2 (2003) 13, https://doi.org/10.1186/1475-925X-2-13.
[56] M. Querol-Vilaseca, M. Colom-Cadena, J. Pegueroles, R. Nuñez-Llaves, J. Luque-Cabecerans, L. Muñoz-Llahuna, et al., Nanoscale structure of amyloid-β plaques in Alzheimer's disease, Sci. Rep. 9 (2019) 5181, https://doi.org/10.1038/s41598-019-41443-3.
[57] I. Raïch, J. Lillo, J.B. Rebassa, C. Griñán-Ferré, A. Bellver-Sanchis, I. Reyes-Resina, et al., Cannabidiol as a multifaceted therapeutic agent: mitigating Alzheimer's disease pathology and enhancing cognitive function, Alzheimers Res. Ther. 17 (2025) 109, https://doi.org/10.1186/s13195-025-01756-0.
[58] N. Reusch, K.A. Ravichandran, B.F. Olabiyi, J.A. Komorowska-Müller, J.N. Hansen, T. Ulas, et al., Cannabinoid receptor 2 is necessary to induce toll-like receptor-mediated microglial activation, Glia 70 (2022) 71–88, https://doi.org/10.1002/glia.24089.
[59] J.P. Rissardo, A.L.F. Caprara, Movement disorders associated with acetylcholinesterase inhibitors in Alzheimer's dementia: a systematic review, Brain Circ. 11 (2025) 9–23, https://doi.org/10.4103/bc.bc_134_24.
[60] S. Ruiz de Martín Esteban, I. Benito-Cuesta, I. Terradillos, A.M. Martínez-Relimpio, M.A. Arnanz, G. Ruiz-Pérez, et al., Cannabinoid CB(2) receptors modulate microglia function and amyloid dynamics in a mouse model of Alzheimer's disease, Front. Pharm. 13 (2022) 841766, https://doi.org/10.3389/fphar.2022.841766.
[61] N. Sánchez-Fernández, L. Gómez-Acero, A. Castañé, A. Adell, L. Campa, J. Bonaventura, et al., A combination of Δ(9)-tetrahydrocannabinol and cannabidiol modulates glutamate dynamics in the hippocampus of an animal model of Alzheimer's disease, Neurother. J. Am. Soc. Exp. Neurother. 21 (2024) e00439, https://doi.org/10.1016/j.neurot.2024.e00439.
[62] M.C. Sañudo-Peña, J. Romero, G.E. Seale, J.J. Fernandez-Ruiz, J.M. Walker, Activational role of cannabinoids on movement, Eur. J. Pharm. 391 (2000) 269–274. ⟨http://www.ncbi.nlm.nih.gov/pubmed/10729368⟩. Accessed May 16, 2018].
[63] R. Saravia, M. Ten-Blanco, M.T. Grande, R. Maldonado, F. Berrendero, Anti-inflammatory agents for smoking cessation? Focus on cognitive deficits associated with nicotine withdrawal in male mice, Brain. Behav. Immun. 75 (2019) 228–239, https://doi.org/10.1016/j.bbi.2018.11.003.
[64] R. Saravia, M. Ten-Blanco, M. Julià-Hernández, H. Gagliano, R. Andero, A. Armario, et al., Concomitant THC and stress adolescent exposure induces impaired fear extinction and related neurobiological changes in adulthood, Neuropharmacology 144 (2019) 345–357, https://doi.org/10.1016/j.neuropharm.2018.11.016.
[65] A.O. Sasmita, E.C. Ong, T. Nazarenko, S. Mao, L. Komarek, M. Thalmann, et al., Parental origin of transgene modulates amyloid-β plaque burden in the 5xFAD mouse model of Alzheimer's disease, Neuron 113 (2025) 838–846.e4, https://doi.org/10.1016/j.neuron.2024.12.025.
[66] M.L. Seibenhener, M.C. Wooten, Use of the Open Field Maze to measure locomotor and anxiety-like behavior in mice, J. Vis. Exp. (2015) e52434, https://doi.org/10.3791/52434.
[67] E. Spangenberg, P.L. Severson, L.A. Hohsfield, J. Crapser, J. Zhang, E.A. Burton, et al., Sustained microglial depletion with CSF1R inhibitor impairs parenchymal plaque development in an Alzheimer's disease model, Nat. Commun. 10 (2019) 3758, https://doi.org/10.1038/s41467-019-11674-z.
[68] N. Stella, THC and CBD: Similarities and differences between siblings, Neuron 111 (2023) 302–327, https://doi.org/10.1016/j.neuron.2022.12.022.
[69] R.S. Toledano, I. Akirav, Cannabidiol prevents cognitive and social deficits in a male rat model of Alzheimer's disease through CB1 activation and inflammation modulation, Neuropsychopharmacol. Off. Publ. Am. Coll. Neuropsychopharmacol. (2025), https://doi.org/10.1038/s41386-025-02213-0.
[70] C. Vázquez, R.M. Tolón, M.T. Grande, M. Caraza, M. Moreno, E.C. Koester, et al., Endocannabinoid regulation of amyloid-induced neuroinflammation, Neurobiol. Aging 36 (2015) 3008–3019, https://doi.org/10.1016/j.neurobiolaging.2015.08.003.
[71] C. Vázquez, R.M. Tolón, M.R. Pazos, M. Moreno, E.C. Koester, B.F. Cravatt, et al., Endocannabinoids regulate the activity of astrocytic hemichannels and the microglial response against an injury: in vivo studies, Neurobiol. Dis. 79 (2015) 41–50, https://doi.org/10.1016/j.nbd.2015.04.005.
[72] Y. Wang, Y. Hong, J. Yan, B. Brown, X. Lin, X. Zhang, et al., Low-dose delta-9-tetrahydrocannabinol as beneficial treatment for aged APP/PS1 mice, Int. J. Mol. Sci. 23 (2022), https://doi.org/10.3390/ijms23052757.
[73] G. Watt, K. Shang, J. Zieba, J. Olaya, H. Li, B. Garner, et al., Chronic treatment with 50 mg/kg cannabidiol improves cognition and moderately reduces Aβ40 levels in 12-month-old male AβPPswe/PS1ΔE9 transgenic mice, J. Alzheimers Dis. 74 (2020) 937–950, https://doi.org/10.3233/JAD-191242.
[74] T. Wyss-Coray, Inflammation in Alzheimer disease: driving force, bystander or beneficial response? Nat. Med. 12 (2006) 1005–1015, https://doi.org/10.1038/nm1484.
[75] S. Yang, Y. Du, X. Zhao, Q. Tang, W. Su, Y. Hu, et al., Cannabidiol enhances microglial beta-amyloid peptide phagocytosis and clearance via vanilloid family Type 2 channel activation, Int. J. Mol. Sci. 23 (2022), https://doi.org/10.3390/ijms23105367.
[76] R. Zhao, W. Hu, J. Tsai, W. Li, W.-B. Gan, Microglia limit the expansion of β-amyloid plaques in a mouse model of Alzheimer's disease, Mol. Neurodegener. 12 (2017) 47, https://doi.org/10.1186/s13024-017-0188-6.